ABSTRACT

INVESTIGATION OF VELOCITY DISTRIBUTION WITHIN HIGH SPEED WATERJET

by
Hong Cao

The aim of this research was to investigate velocity distribution within the water jet at different conditions of jet formation. The water jet (WJ) velocity was measured by the use of Laser Transit Anemometer (LTA) and statistical technique which improved the accuracy of the velocity determination.

The velocities were measured for different diameters of the sapphire nozzle under different water pressures at different axial stand off distances and radial distances across the jet. The experiments performed in this study enabled us to evaluate the effects and conditions of the water jet on the velocity distribution. The acquired results provide information for the nozzle formation and establishing numerical model for predicting the jet properties. Important peculiarities of the jet behavior were also identified.

INVESTIGATION OF VELOCITY DISTRIBUTION WITHIN HIGH SPEED WATERJET

by
Hong Cao

A Thesis
Submitted to the Faculty of
New Jersey Institute of Technology
in Partial Fulfillment of the Requirements for the Degree of
Master of Science in Mechanical Engineering

Department of Mechanical and Industrial Engineering

January 1995

APPROVAL PAGE

INVESTIGATION OF VELOCITY DISTRIBUTION WITHIN HIGH SPEED WATERJET

Hong Cao

Dr. Ernest S. Geskin, Thesis Advisor — Date
Professor of Mechanical Engineering
of the Department of Mechanical and Industrial Engineering, NJIT

Dr. Rong-Yaw Chen, Committee Member — Date
Professor of Mechanical Engineering and Graduate Advisor
of the Department of Mechanical and Industrial Engineering, NJIT

Dr. Zhiming Ji, Committee Member — Date
Assistant Professor of Mechanical Engineering
of the Department of Mechanical and Industrial Engineering, NJIT

BIOGRAPHICAL SKETCH

Author: Hong Cao

Degree: Master of Science in Mechanical Engineering

Date: January 1995

Undergraduate and Graduate Education:

- Master of Science in Mechanical Engineering,
  New Jersey Institute of Technology, Newark, NJ, 1995

- Bachelor of Science in Engineering,
  Shanghai Jiao Tong University, Shanghai, China, 1986

Major: Mechanical Engineering

This thesis is dedicated to
my wife and my parents

ACKNOWLEDGMENT

I wish to express my sincere gratitude to my advisor, Dr. Ernest Geskin, for his guidance, kindness and moral support throughout all my work.

Special thanks to Dr. R. Chen and Dr. Zhiming Ji for serving as members of the committee.

I am thankful to my friends and family members for supporting and encouraging me to complete my studies successfully.

TABLE OF CONTENTS

TABLE OF CONTENTS
(Continued)

Chapter **Page**

LIST OF TABLES

LIST OF FIGURES

LIST OF FIGURES
(Continued)

LIST OF FIGURES
(Continued)

LIST OF FIGURES
(Continued)

LIST OF FIGURES
(Continued)

LIST OF FIGURES
(Continued)

CHAPTER 1

INTRODUCTION

During the past few years, high speed waterjet (WJ) and abrasive waterjet (AWJ) have found more and more extensive application in cutting, drilling and cleaning. As shown in Figure 3, water can be pressurized up to 345 MPa and expelled through a sapphire orifice to form a coherent and high-velocity waterjet .

Abrasive waterjet cutting technology is a natural extension of waterjet cutting. It is shown in Figure 4 that the waterjet enters into a carbide tube. This creates the negative pressure that draws abrasive particles into the tube. The flow turbulence in the tube causes mixing of the water and abrasive particles and forms an abrasive waterjet where part of the waterjet momentum is transferred to abrasive, thus abrasive velocity abruptly increase. As the result, the high-velocity stream of abrasives which can be used to cutting and cleaning is formed. Cutting and cleaning is process in which material removal take place due to the erosion action of particles which strike upon the work surface with high impact velocity.

In order to improve the productivity of waterjet cutting and cleaning, it is necessary to predict the exact nature of the erosion mechanism. The study of surface erosion upon impingement of the WJ and AWJ includes determining the fluid conditions and the direction and velocity of particle striking the surface. Therefore, the determination of the particle velocity at different condition of WJ and AWJ formation is essential for predicting the exact nature of the erosion mechanism involved in the application in cutting, cleaning and drilling.

The condition affecting WJ and AWJ formation can be categorized as follows:

1. Waterjet pressure (P)
2. Sapphire nozzle diameter (d_o)
3. Carbide tube nozzle diameter (d_c)
4. Abrasive material and its size
5. Abrasive mass flow rate (m_a)
6. Carbide tube length (l_c)

In the past, the experimental studies relied on the results of WJ and AWJ application in cutting and cleaning. The research work on special jets, different shapes of the nozzles and their application in industry etc. were also carried out. However, an insufficient effort was dedicated to measuring the stream velocities.

Our research was concentrated on measuring the WJ velocity field distribution along and across the jet of different diameter nozzles and different water pressures and the Laser Transit Anemometer (LTA) was used for measuring the velocity.

The LTA operates by detecting scattered light from small particles as they pass through two focal points of two highly focused laser beams. The distance between these two focal points is known. Velocity is determined by measuring the time taken for the movement of particles from one focal point to other one.

In this research work, the special set up and measurement procedure is very critical for measuring the velocities of particles entrained in the desired region of a high turbulent waterjet; because up to now the LTA application was only limited to low turbulent single-phase or two -phase flows.

CHAPTER 2

DESCRIPTION OF WATERJET CUTTING TECHNOLOGY

2.1 General Description

The first commercial application of the waterjet system was at Alton Box Board, Illinois, in 1971. Cutting with a pure waterjet was limited to non-metal materials, such as food products, rubber, plastics, paperboard forms, etc. This limitation made it impossible to use the waterjet as a universal cutting tools. However, in the early 80's when the abrasive waterjet cutting technology was developed, watejet cutting could be applied to every known material. In recent years, waterjet cutting have been introduced in a large number of industrial application. This technology provides an effective machining method for material shaping, especially for engineering materials, which can not be shaped by conventional machining techniques.

2.2 Advantage of Waterjet Cutting Technology

The substantial advantages of waterjet technologies include following:

1. It is estimated that production cost for hard-to-machine materials constitute a 50% cost of machining using conventional machining technology.
2. The waterjet cuts without heat and thermal distortion because most of the heat generated during the cutting process is removed by the jet. Therefore, the material properties remain unchanged.

3. The processes of cutting produce minimal dust which make operation less hazardous.
4. Cutting of complicated shapes is easily accomplished since the WJ or AWJ is a true point, omni-directional device.
5. Jet reaction forces are relatively low. Therefore, the structural support hardware requirement only must be considered for components and their dynamics, not for cutting force, etc.
6. Waterjet can offer higher cutting efficiency over conventional methods.

2.3 Waterjet Cutting System

The waterjet cutting system is composed of a water preparation unit and a machine work station (Figure 1).

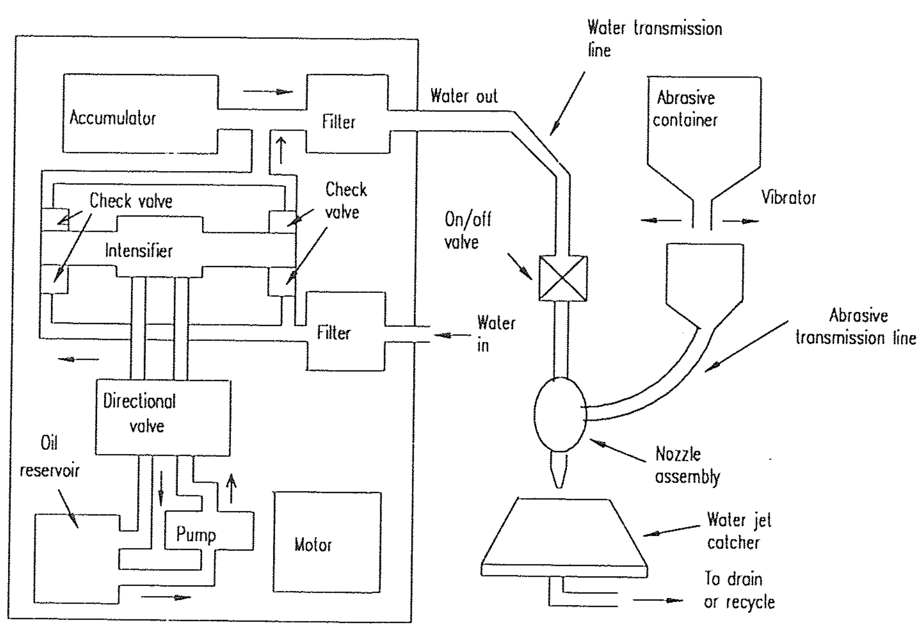

Figure 1 Components of the waterjet cutting system

2.3.1 Water Preparation Unit

The main function of the preparation unit is to feed pure water continuously and to pressurize the water to the required high pressure. This unit consists of booster pump, filter, water softener, prime motor and a oil drive unit (including a hydraulic pump, oil reservoir and valve), an intensifier, accumulator and control, and safety instruments.

1. Booster pump:

   Pumps the water into a low pressure water circuit in order to ensure the continuous flow into the high pressure filters. The softener is used to soften the water and to remove the iron and calcium dissolved solids.

2. Intensifier:

   A hydraulic driven 40 hp oil intensifier is an essential part of the system. It is a sample hydraulically driven reciprocating plunger pump. It develop pressure up to 345 MPa in the water from booster pump. There are two separate circuits for oil and water. The oil circuit is a closed circuit and water circuit is opened. The lower pressure oil is applied alternately to each side of a large piston causing it to move back and forth; reciprocating motion is obtained by valves. The resulting pressure in the small piston chamber is intensified by the ratio of the areas of the two piston, a large piston drive that is connected to a small piston connected to a large piston.

3. Control and safety instruments:

   High pressure water from both sides of the intensifier is discharged to a accumulator where the pressure stabilizes. Since the water at 345 MPa is 12 percent compressed, the water is not discharged uniformly from the intensifier to all piston positions.

Thus the accumulator provides a uniform discharge pressure and flow. A rupture disk is provided as a safety device for the intensifier. For recording oil and water pressure, two pressure gauges are mounted in the oil and water lines, respectively.

4. High pressure water distribution system:

   The high pressure water output of the accumulation is conveyed to the work station through a series of pipes, swivels, flexible joints and fittings. Up to a pressure of 137.90 MPa, the hose can be used to eliminate the need for swivels which greatly simplifies the plumbing. The line pressure drop can be readily calculated on the basis of the number of joints, elbows and the total pipe length.

2.3.2 Work Station

This is the place where the actual experiment is performed. There are four major components as follow: nozzle assembly, abrasive feeder, work place with traversing mechanism and a catcher.

1. Nozzle Assembly:

   The high pressured water is converted into kinetic energy in the nozzle assembly. There are two nozzles housed in the main body and a separate port for the abrasive entrance. The high pressure water supplied from the water distribution line passes through a sapphire nozzle and accelerates to a velocity of 600-800 m/sec. In case of AWJ, the abrasive moves into the side port and mixes with the water from the sapphire nozzle (Figure 5). Here, abrasive particles are accelerated. The performance of the sapphire and carbide nozzles depend on the diameter length, angle of convergence and weight. The entry angle of the abrasive, diameter of port, vertical and horizontal distance between the abrasive inlet and the sapphire nozzle are also typical variables which affect the nozzle design. In this experiment, 6 different sizes of sapphire nozzle #3, #5, #7, #10, #12 and #14 with diameters of 0.0762 mm, 0.127 mm, 0.1778 mm, 0.3048 mm, and 0.3556 mm respectively are used. Schematics of the typical carbide and sapphire nozzles are shown in Figure 4. In a pure waterjet cutting system, the nozzle is a small sapphire orifice with a diameter between 0.1778 mm to 0.3556 mm. In an abrasive waterjet system, we use a sapphire nozzle and carbide tube which has an internal diameter ranging from 0.8636 mm to 1.6 mm. The carbide tubs are made from tungsten carbide.

2. Abrasive Feeder:

   This unit continuously delivers abrasive into the nozzle assembly at a controlled rate. A feed hopper stores 10-180 kg of abrasive and an electron magnetic vibrator tray regulates the flow of abrasive from the hopper. The flow is regulated by changing the applied voltage which, in turn, changes the frequency of vibration. Meantime the suction created in the nozzle assembly draws abrasive from the vibratory tray.

3. Robots and CNC Controlled X-Y positioning Table:

   CNC machine codes can be used to write the program. This program can be loaded into a computer to control water and abrasive flow as well as robot movement.

4. Entrapment, Separation and Drainage:

There is an open tank type catcher that is used to store ejecting high energy jet which contains particles of used abrasive and cut materials. Vacuum tanks are used to collect the water and the particulate slurry, and subsequently to dispose of it.

2.4 Application of Waterjet Cutting

Waterjet cutting can be applied in two aspects: destructive and precision cutting. The destructive application is breaking and removing coal, concert, rock or mineral and cleaning of the objective surface. The objective is to remove the maximum amount of material with minimal consideration of the quality of the cutting edge. Precision cutting applications use the waterjet as the cutting tools. The applications are used in factories and have been continually developed over the last decade.

CHAPTER 3

LITERATURE SURVEY

3.1 Study of Waterjet

Waterjet cutting involves the removal of material by the action of high-velocity water or water with abrasive. There are relatively very few published papers dealing with the velocity distribution in waterjet. Dunne and Cassen [18] investigated the velocity discontinuity and instability of a liquid jet having a velocity higher than the sound speed. Schlieren photography was used in his study to observe the development of a jet and to determine its velocity. Semerchan [19] investigated the distribution of momentum in a continuous liquid jet of supersonic velocity. The average velocity of jet was determined from the measurement of the discharge rate of water and compared with the value calculated from Bernoulli's equation. Measuring a number of the flow by use of Schlierrn photography, Kinvshita studied the compressibility of the waterjet.

3.2 Velocity Measurement of the WJ and AWJ

The characteristics of water flow in air were investigated by Yanaida and Ohashi [7]. The authors give a theoretical analysis of the breakup characteristics of a high-speed waterjet in air and verified their results by using the electric method and laser velociment. They showed that the statistical variation of break up length is described in the Gaussian distribution. It was found that velocity is constant in the continuous flow region, diminishes slightly in the droplet diffused flow region and drops abruptly in the diffused flow region. They were unable to measure the axial velocity in the diffused flow region because of the jet instability.

Hishida, Nakano and Maeda [8] used an experimental method to investigate the turbulent structure of a liquid-solid two-phase jet to examine models of the phases. The authors observed that the liquid velocity increment in a two-phase flow due to slip velocity between the solid and liquid phases is larger in the down stream direction.

The ratio of velocity fluctuation and turbulent Reynolds shear stress to local velocity difference between the centerline and the outer flow region decreases due to the existence of particles.

Givler and Mikatarian [9] have developed a fluid-particle fluid model. Their primary concern was to calculate the concentration of solid particle within a flow field in order to indicate the initiation of a particle plug.

Swanson [10] determined the abrasive particle velocity by experimental methods. In this experiment, conventional garnet sand mixed with magnetic particles of comparable size was injected into a conventional waterjet and the resultant cutting streams directed by a pair of current-carrying coils spaced at a fixed distance apart. The velocity can be determined by measuring the time between the signal response from each of the coils. It was found that the particles which enter the jet at periphery tend to stay at the periphery without further penetratrtion. Their work shows that the advantage of abrasive waterjet cutting can be achieved if a more effective means of accelerating the abrasive particles can be developed .

Edwards [11] developed a mechanism which can dispersed rapidly droplets separating from the jet boundary in air from the central core in a manner detrimental to jet velocity based on Magnus-effect.

Davies [12] has done experiments concerned with the anatomy and impact characteristics of large scale waterjets. These authors used 3 different nozzles in experiments. Velocity decay along the jet from nozzle to the impact site was determined by measuring the relative displacement of the packets between subsequent frames of a film.

Janakiram and Syamala Rao [13] developed a computer study of the flow pattern that calculated velocity distribution during the impingement of a plain jet on a rigid target material. Using a finite difference technique, the author solved the equations of motion for incompressible and viscous flow in cylindrical coordinates.

They used different plain jets ranging in diameter from 4 mm to 12 mm and also cavijets from 7.59 mm to 11.6 mm in diameter in order to study the growth of area of erosion due to the impingement of the plain jets with varying jet velocities

Arthur L. Miller and John H. Archibald [14] measured a quasi-instantaneous abrasive particle velocity in a three-phase abrasive jet cutting system by using an electronic velocimeter. A small portable electronic velocimeter was designed which can be fitted over the outside of a collimating pipe and slides easily to any axial position along the pipe. The velocimeter consists of two energized electromagnetic coils placed at a known distance apart, each wrapped with a secondary object coil. Any object which has magnetic permeability will cause a transient disturbance of the magnetic flux lines as it moves through either of these primary coils which carry approximately 3/4 amp at 2 volts. Such a disturbance induces a small transient voltage signal in the respective secondary coil, which can be captured by the oscilloscope. The velocity of the particle can then be determined by measuring the time increment between the two signals.

A velocity profile for the abrasive parcels was constructed and momentum transfer in the system was analyzed by using the measured data. It was shown that particle acceleration is strongly dependent upon particle specific gravity and weakly dependent on particle size. The momentum transfer from the fluid to the abrasive particles would reach momentum equilibrium sooner for lighter abrasive particles.

CHAPTER 4

THEORY OF MEASUREMENT AND EXPERIMENT PROCEDURE

4.1 Introduction

The present study is concerns itself with the experimental investigation of a velocity field in the waterjet. The experiment involves in using the Laser Transit Anemometer (LTA) Technique to measure the velocity distribution of waterjet along and across the jet.

Tests were carried out in the Waterjet Machine Laboratory in the Mechanical Engineering Department of New Jersey Institute of Technology.

The waterjet cell used for the experiment was manufactured by Ingersoll Rand. It has a 3 axis controlled with a Allen Bradley mill controller. It consists of a water preparation unit, a nozzle assembly, an abrasive feed, a work place with a traversing mechanism and a catcher (Figure 1).

4.2 Laser Transit Anemometer Technique

Laser Transit Anemometer (LTA) provides a effective method of nonintrusive measurements for obtaining flow field information [5,6,15,16,17]. Particles in the flows supply scattering centers for the incident light. There are two common techniques for optically coding the measurement region. The first is Laser Doppler Anemometer (LDA) which is dependent on varying fringe patterns [1-3]. Knowing the fringe spacing and the detected frequency of particles passing through, the measurement region can determine the velocity component normal to the fringes. The second is using closely spaced two spots in measurement region where the flow direction is parallel to the axis connecting the two spots. The velocity is obtained from the time-of-flight (TOF) of the particles passing the two spots. The distance between the two foci is 300-600 μm which is far greater than the distance between the fringes (Figure 6).

The signal obtained from TOF system yield two pulses separated by the transit time when the particles pass through the two focal points in measurement region. The velocity of the particles along the two focal points can be calculated by knowing the peak-to-peak time of flight and the distance between the two foci spots (Figure 7). But unfortunately, most particles do not travel directly from one focus to other focus. There four possible cases for the motion of particles (Figure 2). The details of prevention of incorrect data will be discussed in Art 4.7. For homogeneous turbulence, if the distance between the two foci, L, is small enough, the turbulence parameters within distance 2L can be considered as constant. The average distance between particles is assumed to be far greater than L. The direction of flow is always considered from one focus towards the other focus.

4.3 Description of Waterjet Machine

A special system of components has been developed in order to pressurize the water. The equipment used in this research is the stream line waterjet cutter manufactured by the Ingersoll-Rand Co. which is divided into four major part: the hydraulic unit, the nozzle body, the abrasive feeding system and milling work cell.

The waterjet system provides three-dimensional cutting with feed speeds up to 3276 in/min and with positioning accuracy 0.0001 in. The work cell components includes:

1. A gantry which is driven with a precision rank and pinion with a dual-side accomplished through a large diameter drive shaft to avoid the problem of a "walking gantry".
2. Stainless steel Thompson rods to enable operation in the most advance conditions
3. Hardened and ground ball screws for Y and Z axis movement.
4. The Allen Bradley 8400 mill controller which provides the following feature:
    a. programmable acceleration / deceleration ramps
    b. teach pendent programming
    c. feedback failure detection
    d. bubble memory.
    e. on line edit capability.

4.4 Experiment Instrumentation and Apparatus

The measuring system used in this study has been developed by Dantec Electronic Co. and a 15 mw He-Ne Laser is used as the light source. The system consists of an optical head and a data processing system.

1. Optical Head:

   The set up of the optical head is illustrated in Figure 8. The two polarizes P1 and P2 make it possible to rotate the internal parts of the system which is the beam plane and the direction of the flight particle. The beam splitter BS1 receives the source light and creates the beams. The two beams are focused by the lens systems to form the measuring volume and the image of two focal points (Figure 9). The distance between the two focus points is 449 μm. The image of the two points is received by the same lens system and transmitted via the mirrors M1 and M2 to the beam splitter BS2. The beam splitter BS2 is rotated together with BS1 to keep alignment. The scattered light, generated by a particle passing through the measuring volume is detected and changed into the voltage signals by the photomultiplier PM. Then the signals are transmitted to the data processing system to determine the particle velocity by measuring the time period between the signals. which is shown in Figure 7.

2. Mechanics:

   The built-in traversing mechanism is compatible with other Dantec Traversing Mechanisms. The calibration factor for the optical encoder is 150 plus per degree.

3. Alignment:

   There are bench alignment and pinhole adjustment. In Bench Alignment, vertical and horizontal bench position are adjusted to obtain transmitted beams of uniform intensity over the exit aperture. In pinhole alignment, a pinhole with a black and non-diffuse surface, which is position in measuring volume, is adjusted.

4. Data Processing System:

   The data processing system of the LTA measurement is consist of :

   Counter Processor, Oscilloscope and Computer (Figure 10).

The 55L90A Counter Processor receives the voltage signals from the photomultiplier in the optical head and conveys these signals both in analog form to the oscilloscope and also in digital form to mean computer. The function of the computer is to determine the time period between two successive signals (peak-peak) which are fed to the Counter Processor and then calculate the velocity.

$$V = d / t \tag{4.1}$$

where d is the distance between the focal points and t is the time period between two successive signals.

These velocity values are continuously displayed on the LTA Counter for every time interval.

5. Nico-320 Nicolet Oscilloscope:

The Nicolet 2-channel digital oscilloscope was used to view the signal from measurements in this study. It has the following functions:

Display:	5-inch, high definition
Save Reference:	Save one reference signal for each channel
Trigger:	
a. Modes	Auto/ Norm
b. Coupling:	AC/DC
c. Slop:	+ or -
d. Soure:	Channel A, Channel and External
Numeric	
a. YT Display Mode:	Time and voltage plus channel identifier.

b. XT Display Mode:	X-volts and Y-volts plus channel identifier.
Expansion	Cursor-interactive
a. YT (Horizontal):	Up to X400
b. YT (Vertical) :	Up to X10
c. XY (Both Axes):	Up to X10
Bubble Memory	
a.Bubble Memory Type:	One megabit bubble memory cassette.
b. Capacity/Cassette:	21-4K pt wave forms and 20 linked functions.
c. Write Protection Manual	
d. Autocycle:	Available though function menu.
Digital I/O:	
a. Interfaces Available IEEE-488 (GPIB), RS-232c,	
	Digital plotter controller (RS-232, IEEE-488)
b. IEEE-488 (GPIB):	Bi-direct, upto 15k bytes/sec output ASCII or binary.
c.RS-232C:	Bi-direct, upto 19.200 baud, ASCII or printable binary.
d. Transfer Time (min, 4k)	
1. GPIB Binary output:	1.5 seconds
2. RS-232 Binary output:	18 seconds

4.5 Measurement Procedure

4.5.1 Mounting of Nozzle Body

It is important to mount the sapphire before starting the experiment nozzle. Therefore, the following procedure was developed:

a. The new nozzle was first checked for manufacture defects.

b. The nozzle body was removed from the robot and then cleaned .

c. A new sapphire was placed in the nozzle body.

d. The intensifier was turned on at low pressure 25-35 MPa and the jet stream was examined that it was established the jet is not scattered.

e. Intensifier was set to Auto and to a high pressure to observe that the jet has the normal geometry. If the jet was not satisfied, operations a. to d. was repeated.

4.5.2. Velocity Measurement

In this experiment, the water particle velocity was measured by using the Laser Transit Anemometer. Both axial and transverse jet velocity were measured at six different sizes of the sapphire nozzles; were used at different stand off distances and different pressures.

a. Axial water velocity measurement was carried out under different pressures:

Under different pressures of 68.95 MPa, 137.90 MPa, 206.86 MPa and 310.28 MPa, the nozzles #3, #10 and #14 (diameter 0.0762 mm, 0.254 mm and 0.3556 mm respectively) were used at stand off distance of 0.5 mm, 3 mm, 6 mm, 12 mm, 25 mm, 50 mm, 100 mm, 150 mm, while the nozzles #5, #7 and #12 (diameter 0.127

mm, 0.1778 mm and 0.3048 mm) were used at stand off distances of 0.5 mm, 12 mm and 50 mm.

1. Firstly, a sapphire nozzle was attached to the nozzle body and the coherence jet at low pressure was checked.
2. The foci of the concentrated laser beam was focused on the low pressure jet and a 10x magnifying glass was maintained behind the jet in order to observe the location between the laser light and jet. If two beams pass right through the center of the jet, there will be two parallel beams on the board (Figure 11). This indicates that the jet is aligned at the center with the focused plane.
3. The LTA was connected with the signal processing counter, the mean velocity computer, and oscilloscope.
4. The counter should be set to the operation mode. The mode selector was put in the transit position. The computer accuracy was set off. The digital high pass was turned on. The maxim time was first selected high enough to be accepted. In other hand, the maxim time was selected to be as short as possible in order to reject most of the false events. The low-pass frequency was reduced until a pulse height reduction and pulse broad was observed. The high-pass was increased until an overshoot of 30-60 % was obtained. In the experiment, selecting 16 MHz for the low pass and 1 MHz for the high pass will give optimal results. The scale factor of 8396 was selected. The ensemble width was kept at 1 and thumb wheel position at 1 or 2 according to the desired velocity

range. Amplifier gain, threshold window and voltage reduction buttons remain all released.

5. The oscilloscope was connected with the counter output to observe the direct response of the signals. The channel B was made active. DC offset voltage was reset to zero. Time per point was selected as 100 ns-500 ns and channel voltage was set to 300 mv. The horizontal division represents 1 micro second and the vertical division represents 75 mv. The AC signal was stored by selecting the normal operating mode.
6. After setting the LTA counter and oscilloscope, a NC program was loaded into the WJ machine for the water flow at a certain pressure of 68.95 MPa, 137.90 MPa, 206.86 MPa and 310.28 MPa for 2000 second without robot movement.
7. While the program was executing, digital display windows on the counter show the velocity in m/sec continuously and the oscilloscope also receives signals. All signals are recorded instantly.
8. Press the hold last and let oscilloscope display the data frozen in memory. When two peaks above 150 mv appear and other peak are below +/- 50 mv, the oscilloscope is receiving satisfactory signals. These signal were considered as valid and then were stored. At this moment about 150 data points are recorded from the counter. The data were statistically analyzed to get the average velocity at the station.

9. Nozzle was moved to the next stand off distance and above steps 2 through 8 were repeated. The experiment other stand off distance were conducted in a similar manner.
10. The water pressure was changed to another value and steps 2 though 9 were repeated to measure velocities along jet axis under different water pressure.

b. Velocity distribution across the jet:

The velocity distribution across the jet was measured for the sapphire nozzle with pure water. The sapphire nozzle #10 was used in the present study under the pressure of 310.28 MPa. The velocity distribution across the jet was measured at three different stand off distances of 0.5 mm, 12 mm and 25 mm.

First, two parallel beams of laser light were focused at the center of the jet and then the jet was moved towards the left by a step of 0.127 mm. At each radial position, the velocity was measured in the same way as it is described in Art 4.5.2 (a). The movement of jet towards left step by step and measuring the velocity were continued until the noise level was kept in +/- 50 mv and no random two peaks over other noise signal occur. Then the nozzle was moved to next station and measurement procure of across the jet at this stand off is same as it was described above .

4.6 Experimental Techniques

Some details involved in the experiment are described in detail to ensure the experiment success.

4.6.1 Focus Point Finding

At the first, two concentrated laser beams were focused on the low pressure jet with a 10X magnifying glass put behind the jet in order to observe the laser light stripe. Then using the hand wheel on the control panel, the jet center was aligned with the two parallel beams. For Y direction, when two laser beams hit low pressure waterjet, it will project two horizontal parallel light stripes on background screen. a hand wheel will be used to adjust the Y direction position of jet until the projecting lights is the same length and brightness to each other. For the X direction, focusing distance is 600 mm which is derived by using a ruler rugged. The hand wheel on control panel on x direction assure the accurate focusing distance on X direction in order to find focus point.

4.6.2 CNC System Programming

Our machine is a two and a half axis waterjet work cell. Its controller limits 300 second turn on without robot movement. In order to increase the time limit to 2000 second we have to add the same line of time control as of the CNC program.

After aligning the focusing point with the waterjet or the finished every measurements at given stand off distances, press the "shift" and "stop" button together to turn off the intensify and cancel the executive program in order to avoid the lost of focusing; because when pressing "emergency stop" bottom, the robot will move a little and the focusing will be lost.

4.7 Validation of the Data

The LTA operates by detecting scattered light from small particles as they pass through two focal points of the laser beams. As shown in Figure 12, when a particle pass through the first focal point, a stating pulse is generated; then the stop pulse is generated by the same particle passing through the second focal point. The velocity is determined by measuring the time of the flight of particle moving from one focal point to other focal point of beams. However, in a turbulent flow, not every particle passing through the measuring volume meets both focal points of the beams and generates start-stop pulses. There are four possible cases regarding the travel of particles and generation of voltage signal as shown in Figure 2.

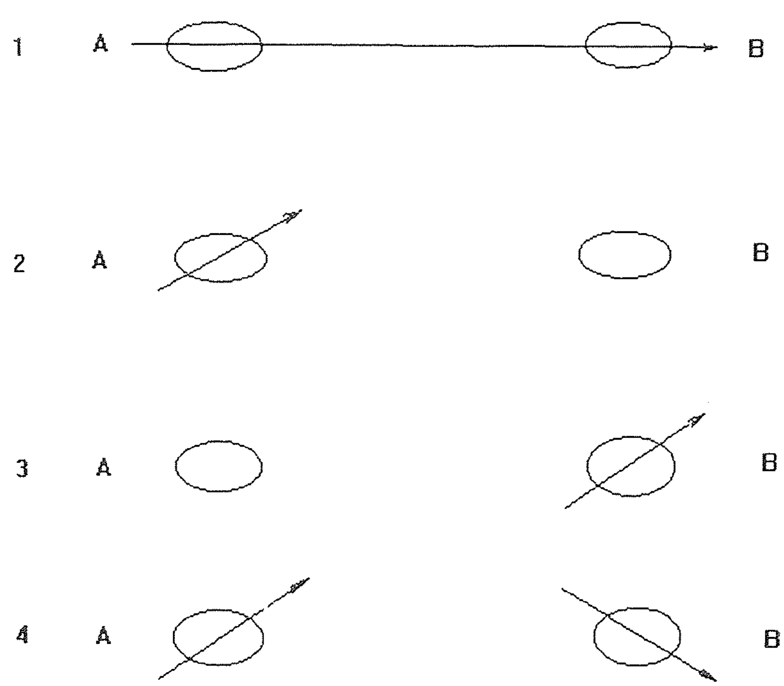

Figure 2 The four possible cases relating to the travel of particle

Case 1 A particle travels directly from the first focus A to the second focus B within certain time T.

Case 2 After a particle passes through focus A, no other particle passes through focus B during the time T.

Case 3 After a particle passes through focus B, no other particle crosses focus A during time T.

Case 4 After a particle passes through focus A (or B) another particle crosses B (or A) during time T.

Only the time interval resulting from the pulses in case 1 is correct representation of particle velocity.

The pulse generated in case 2 and case 3 is unacceptable by the computer since there is no successive peaks within the set time T.

The velocity getting from case 4 is not correct particle velocity since the two pulse is generated by different particles. The occurrence of this case is due to the following factors:

1. The mean distance between particles is smaller than the distance between two focal points.
2. The two focal points are not aligned along the direction of the flight of the particles.

The correct and false time intervals occurring in case 1 and case 4 can not be identified directly by Data Processing System. However, the correct data has principal probability if the occurrence of incorrect data is much less than the occurrence of the correct one. So that the experimental data collected can be analyzed statistically (using

Statistical Analysis for Engineers software) and as shown in figure 13, distribution of occurrence probability is obtained.

This curve consists of two regions. The data with higher occurrence probability are distributed over the horzontal line L and in region A and are considered as the correct data. The data with lower occurrence probability are distributed below the horizontal line L and represent the resulting noises. The arithmetic mean velocity from all correct data can represent the particle velocity.

In general, it is possible to reduce the occurrence of false time interval by setting a correct experiment.

1. The distance between the two focal points is kept shorter then the mean distance between the particles.
2. The two focal points are aligned as perfectly as possible with the direction of the flight particles.

The suitable distance between the two-foci is in the design of optical head of LTA system. As reported in [16], the distance should be in range 0.3 mm to 0.5 mm in order to secure a satisfactory measurement. In our measurement study this value is 0.449 mm and is found to be suitable for our measurement.

CHAPTER 5

EXPERIMENTAL RESULTS AND DISCUSSION

In this study, velocity measurements along and across the jet were conducted under different water pressures for waterjet by LTA. Velocity distribution measurements along the jet axis for the nozzles #3, #5, #7, #10, #12 and #14 (diameter 0.0762 mm, 0.127 mm, 0.1778 mm, 0.254 mm, 0.3048 mm and 0.3556 mm) were carried out at the pressures of 68.95 MPa, 137.90 MPa, 206.86 MPa and 310.28 MPa for each nozzle. In velocity distribution measurement across the jet at three stand off distances, sapphire nozzle #10 is used and the discharge pressure is maintained at 310.38 MPa. About 150 data points were processed by using "Statistical Analysis For Engineers" package.

The percentage of occurrences of velocities on the axis of the jet at two stand off distances is shown in Figures 14-25. The mean occurrence range gives the velocity at that station. We noticed that there are few occurrence in velocities far from the highest occurrence zone which are generated by noise and deviant signals. These occurrence was so low that they did not affect the determination of the actual velocity at that station. From Figures 14-15, it was noticed that the peaks occur at higher velocity at or near stand off distance from the nozzle tip than at far stand off distance which is due to the velocity decrement. Figures 14-17 are constructed for nozzle #3, Figures 18-21 for nozzle #10 and Figures 22-25 for nozzle #14.

The percentage of occurrence of velocities across the waterjet at two radial distance from center are shown in Figures 26-28. From these figures, we notice that the peak occurs at the higher velocity at center than that at the far radial distance. This is due to the velocity decrement being a little bit along radial direction.

Tables 1-7 indicate velocity values of six different nozzles diameter along axial direction under four different pressure and one nozzle diameter in radial direction at three stand off distances.

Velocity obtained from the percentage occurrences at each stand off distance for nozzles of #3, #10 and #14 (diameter 0.0762 mm, 0.254 mm and 0.3556 mm) under water pressures of 68.95 MPa, 137.90 MPa, 206.86 MPa and 310.28 MPa are shown in Figures 29-40. These fitting curve graphs indicate that the rate of the velocity decreases along axial direction under certain pressure.

Figures 41-44 show the velocity distribution along the axial of a jet for different nozzle under certain pressure of 68.90 MPa, 137.90 MPa, 206.86 MPa and 310.28 MPa. These graphs indicate both the velocity decrease in the axial direction and the velocity dependence on the sapphire nozzle diameter. The larger the sapphire nozzle diameter, the lower velocity is.

In Figures 45-47, it is showed that velocity distribution on axis for certain nozzles of #3, #10 and #14 under pressures of 68.90 MPa, 137.90 MPa, 206.86 MPa and 310.28 MPa .These data and graphs indicate that the velocity decreases at the fixed stand off distance with decrement of pressure.

At the tip of nozzle, the correlation between the waterjet velocity and the pressure is as fellows:

$$V = K\sqrt{P} \tag{5.1}$$

where V is the waterjet velocity at an exiting of nozzle tip. (m/s)

K is parameter

P is water pressure (Pa)

The first column values in each table indicate the velocities at the nozzle exiting under different pressure for each nozzle size. Figure 75 shows the correlation between parameter K and nozzle diameter and water pressure. From these measurement data, we can get a practical experimental parameter K for nozzle #3, #5, #7, #10, #12 and #14 by the use of arithmetic mean method. That is K_3=0.0389, K_5=0.0386, K_7=0.0379, K_{10}=0.0374, K_{12}=0.0374 and K_{14}=0.0364 where K_3 is parameter for nozzle #3, K_5 for nozzle #5, K_7 for nozzle #7, K_{10} for nozzle #10, K_{12} for nozzle #12 and K_{14} for nozzle #14.

Figures 48-50 show radial velocity distribution at various stand off distances.

Figures 51 shows radial velocity distributions at three different stand off distances. It is very difficult to measure velocity near the boundary of the jet because the velocity received by LTA at the boundary does not confirms single particle motion condition. The presented velocity distribution are recorded in the region where the LTA confirms single particle motion. In these figures, it is indicated that the velocity decrements in the radial direction. These distribution corresponds to the Gaussion velocity distribution.

Figures 52-54 show the normalized velocity distribution along jet axial at two different stand off distances for three nozzles of #3, #10, #14 under different pressures.

Figure 55 shows the normalized velocity distribution across the jet at different stand off distances.

Tables 8-13 indicates V^2/P value at different stand off distance x/d_0 and P is the water pressure. The value V^2/P indicate effect of energy transfer during fluid acceleration and energy loss.

Figures 56-67 fitting curves show V^2/P value distribution at different stand off distance x/d_0 for three nozzles diameter under four different pressures. These graphs indicate V^2/P decrease along axial downstream direction.

Figures 68-70 show axial V^2/P distribution for nozzles of #3, #10 and #14. From these graphs, we notice that V^2/P increase with increment of P at certain stand off distance except for P=206.80 MPa.

Figures 71-74 show effects of nozzle diameter on axial V^2/P distribution at different stand off distance x/d_0 under certain pressure. These graphs indicate that V^2/P increases with nozzle diameter decreasing.

CHAPTER 6

CONCLUSIONS

Velocity measurement for the waterjet by Laser Transit Anemometer has been established. From the acquired data, we can draw the following conclusions:

1. At constant pressure, an increase of the sapphire nozzle diameter causes an decrease of the velocity.
2. With the increase of the pressure, the velocity also increases. The correlation between velocity at exiting of nozzle tip and pressure can be formed as the experimental formula of $V=K\sqrt{P}$. K is depend on nozzle structure parameter. The diameter is most principle parameter in these parameter.
3. The velocity decrease with increment of axial stand off distance.
4. The velocity decreases across the jet in radial direction.
5. V^2/P decrease with increment of axial stand off distance and increase with decrement of nozzle diameter.
6. The following peculiarities in the velocity distribution were observed . The pressure change from 206.86 MPa to 137.90 MPa effect the axial jet velocity much weaker than the pressure change from 310.38 MPa to 207.86 MPa and 137.90 MPa to 68.95 MPa. This peculiarity has been observed for all sapphire diameters. The criterion V^2/P characterizing the energy conversion in the nozzle has the highest value at P=310.38 MPa and lowest at P= 68.95 MPa. However, the value of this criterion at

137.90 MPa is higher than that at 206.86 MPa. The peculiarities above will be studied during our following work.

7. The acquired database will be used for the study of peculiarities in the development and behavior of the high speed waterjet.

APPENDIX

TABLES AND FIGURES

Table 1 Axial velocity (m/s) distribution for nozzle diameter d_o= 0.0762 mm

Pressure (MPa)	Stand off Distance (mm)						
	0.5	6	12	25	50	100	150
68.95	285	282	278	260	240	217	176
137.90	479	463	451	434	402	372	329
206.86	554	539	522	483	446	387	352
310.28	754	737	709	672	604	562	504

Table 2 Axial velocity (m/s) distribution for nozzle diameter d_o= 0.254 mm

Pressure (MPa)	Stand off Distance (mm)						
	0.5	6	12	25	50	100	150
68.95	275	261	245	229	214	186	159
137.90	453	441	440	421	372	340	293
206.85	530	489	478	462	398	363	331
310.38	735	692	682	663	565	526	461

Table 3 Axial velocity (m/s) distribution for nozzle diameter d_o= 0.3556 mm

Pressure (MPa)	Stand off Distance (mm)						
	0.5	6	12	25	50	100	150
68.95	269	246	229	219	201	178	143
137.90	441	432	426	402	364	331	293
206.85	497	481	468	447	386	358	321
310.28	730	685	658	653	557	517	457

Table 4 Axial velocity distribution at three stand off distances
for nozzle diameter d_o= 0.127 mm

Pressure (MPa)	Stand off Distance (mm)		
	0.5	12	50
68.95	284	268	225
137.90	467	449	396
206.85	545	513	415
310.28	751	709	597

Table 5 Axial velocity (m/s) at three stand off distances
for nozzle diameterd_o= 0.1778 mm

Pressure (MPa)	Stand off Distance (mm)		
	0.5	12	50
68.95	280	246	213
137.90	460	446	379
206.85	529	487	402
310.28	741	679	570

Table 6 Axial velocity (m/s) at three stand off distances
for nozzle diameter d_o=0.3048 mm

Pressure (MPa)	Stand off Distance (mm)		
	0.5	12	50
68.95	273	237	205
137.90	453	431	374
206.85	518	476	396
310.28	734	667	563

Table 7 Velocity (m/s) distribution across jet at three stand of f distances
pressure= 310.28 MPa, nozzle diameter d_o= 0.254 mm

Stand off Distance (mm)	Radial Distance From Nozzle Axis (mm)					
	0	0.127	0.254	0.381	0.508	0.635
0.5	735	726	706	690	655	-----
12	682	670	655	629	619	586
25	663	651	642	616	591	577

Table 8 Axial V^2/P ($\times 10^{-3}$) distribution for nozzle diameter d_o= 0.0762 mm

Pressure (MPa)	Stand off Distance x/d_o						
	6.65	78.74	153.48	328.48	656.16	1312.34	1968.50
68.95	1.178	1.153	1.120	0.980	0.835	0.664	0.449
137.90	1.663	1.554	1.474	1.365	1.171	1.004	0.785
206.86	1.483	1.404	1.317	1.127	0.961	0.724	0.599
310.28	1.832	1.750	1.620	1.455	1.175	1.018	0.818

Table 9 Axial V^2/P ($\times 10^{-3}$) distribution for nozzle diameter d_0= 0.254 mm

Pressure (MPa)	Stand off Distance x/d_0						
	1.968	23.62	47.24	98.43	196.85	393.70	590.55
68.95	1.096	0.988	0.871	0.761	0.664	0.502	0.367
137.90	1.488	1.410	1.404	1.285	1.004	0.838	0.623
206.85	1.357	1.156	1.104	1.031	0.766	0.637	0.529
310.38	1.740	1.542	1.499	1.416	1.028	0.891	0.685

Table 10 Axial V^2/P ($\times 10^{-3}$) distribution for nozzle diameter d_0= 0.3556 mm

Pressure (MPa)	Stand off Distance x/d_0						
	1.41	16.87	33.75	70.30	140.61	281.21	421.82
68.95	1.049	0.878	0.761	0.696	0.586	0.460	0.297
137.90	1.410	1.353	1.316	1.172	0.961	0.794	0.623
206.85	1.194	1.118	1.059	0.966	0.720	0.620	0.498
310.28	1.717	1.512	1.395	1.374	1.000	0.861	0.673

Table 11 V^2/P ($\times 10^{-3}$) at axial three stand off distances
for nozzle diameter d_0= 0.127 mm

Pressure (MPa)	Stand off Distance x/d_0		
	3.94	94.49	393.70
68.95	1.169	1.041	0.734
137.90	1.582	1.462	1.137
206.85	1.436	1.272	0.833
310.28	1.817	1.620	1.148

Table 12 V^2/P ($\times 10^{-3}$) at axial three stand off distances for nozzle diameter d_o= 0.1778 mm

Pressure (MPa)	Stand off Distance x/d_o		
	2.81	67.49	281.21
68.95	1.137	0.878	0.658
137.90	1.534	1.442	1.042
206.85	1.353	1.147	0.781
310.28	1.769	1.486	1.047

Table 13 V^2/P ($\times 10^{-3}$) at axial three stand off distances for nozzle diameter d_o=0.3048 mm

Pressure (MPa)	Stand off Distance x/d_o		
	1.64	39.37	164.04
68.95	1.081	0.815	0.609
137.90	1.488	1.347	1.014
206.85	1.297	1.095	0.758
310.28	1.736	1.433	1.022

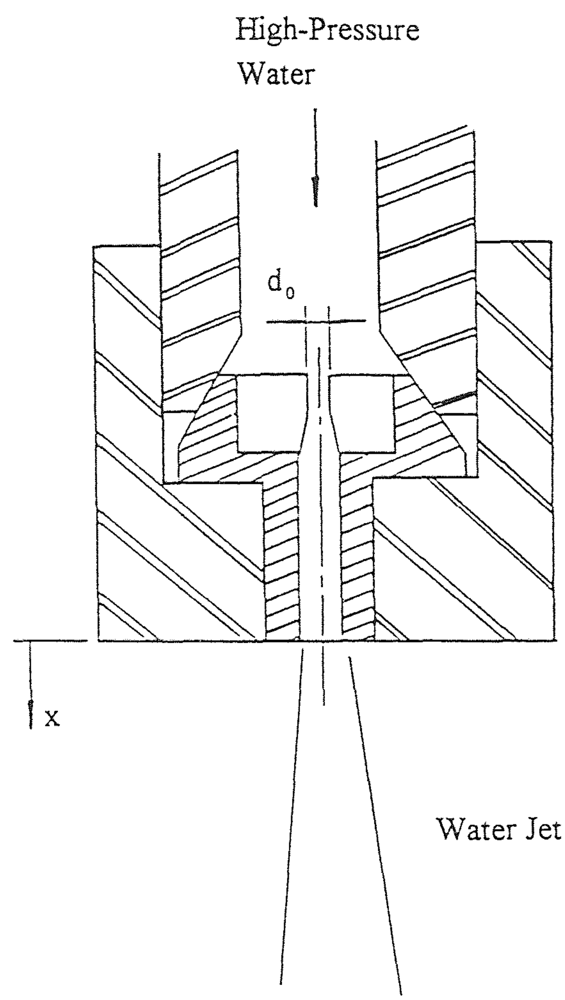

Figure 3 Schematic of sapphire nozzle with water flow

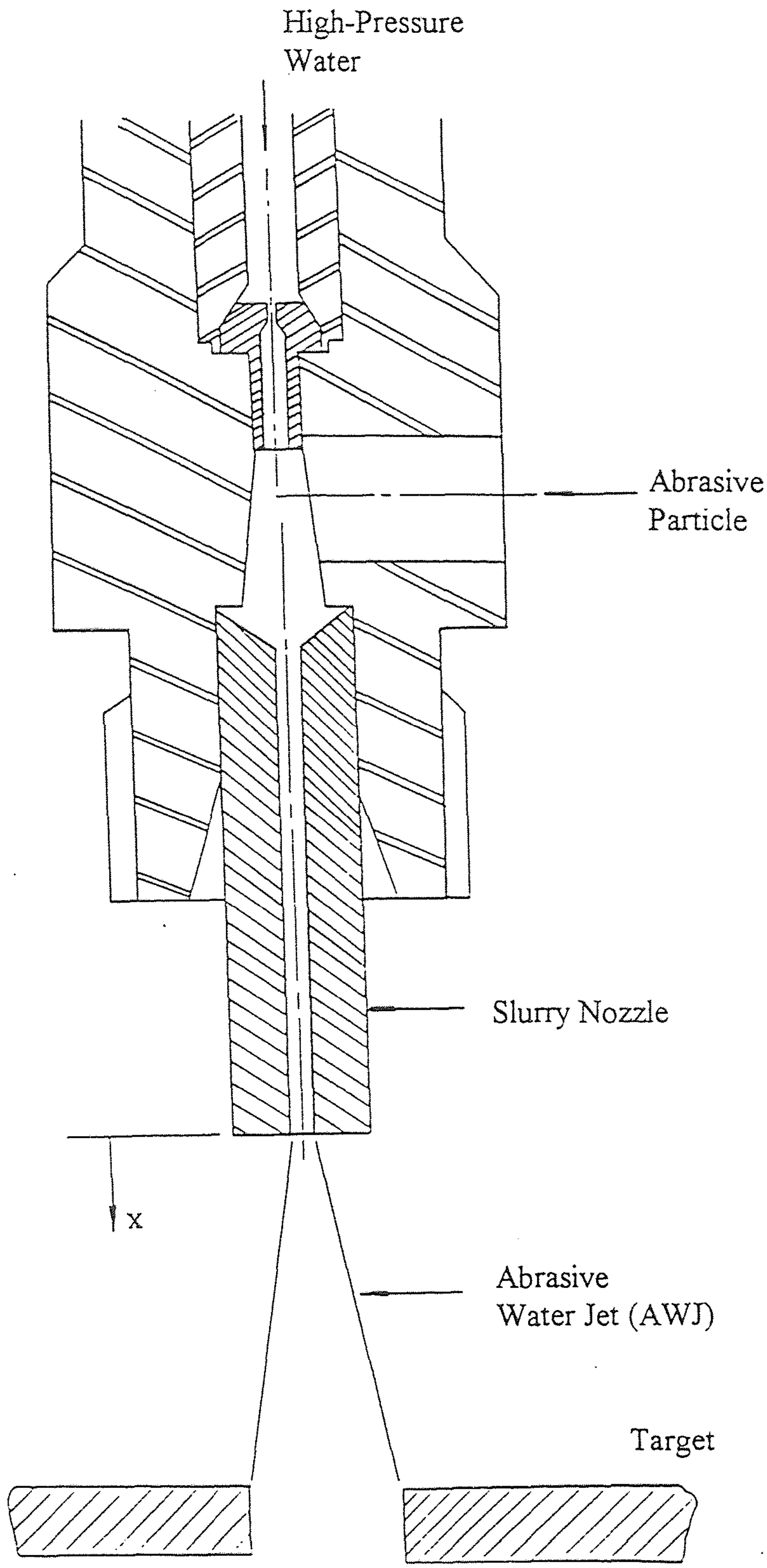

Figure 4 Schematic of carbide nozzle with flow

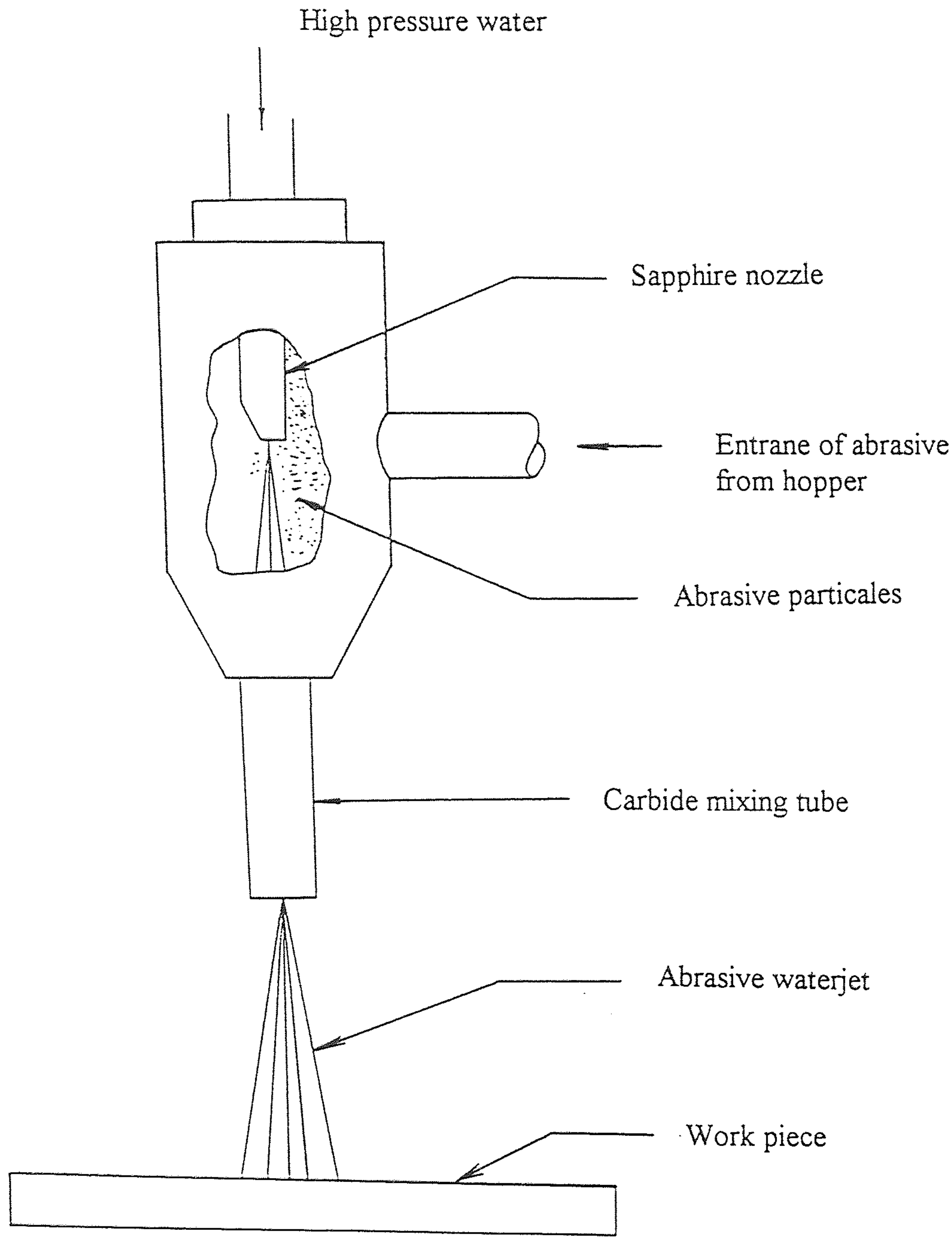

Figure 5 Schematic of the jet formation and jet-work piece interaction

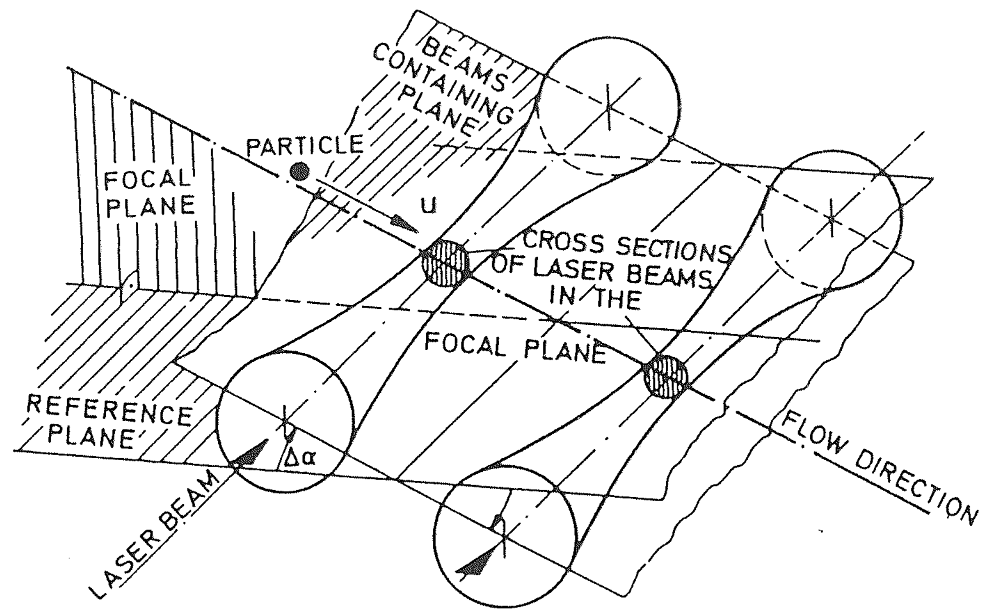

Figure 6 Schematic of the LTA measuring volume

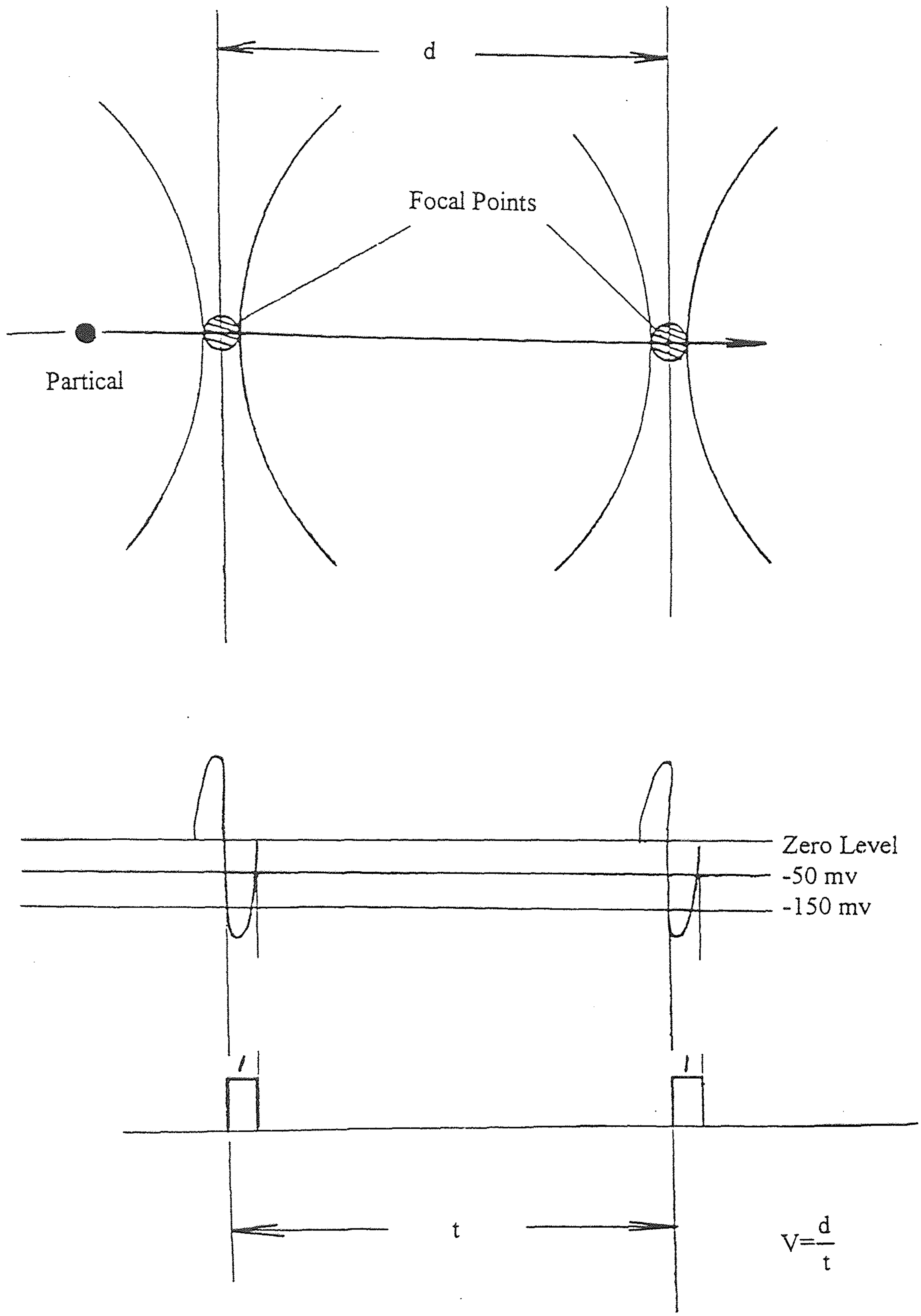

Figure 7 Wave form of output signals for digitization

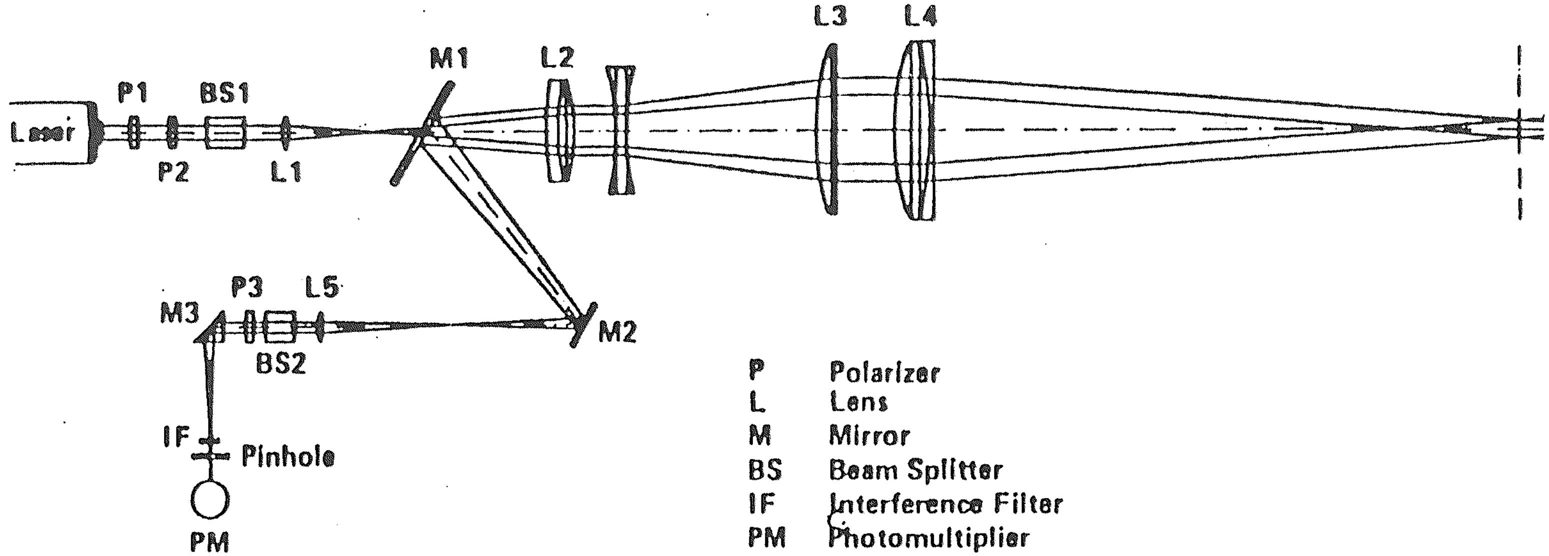

Figure 8 Schematic of the optical head of LTA

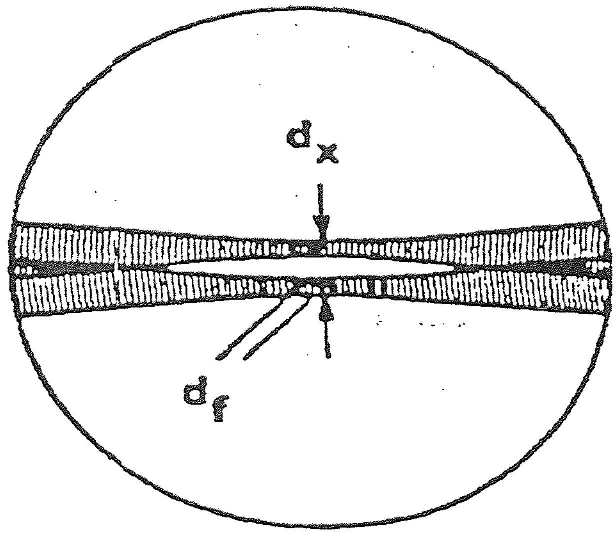

Figure 9 Measuring volume of LTA

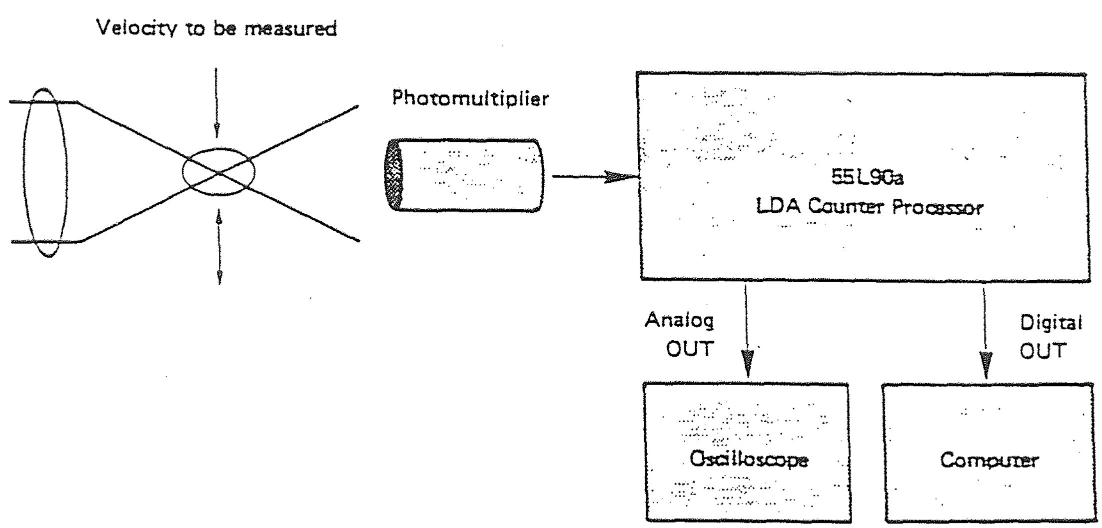

Figure 10 LTA with counter processor

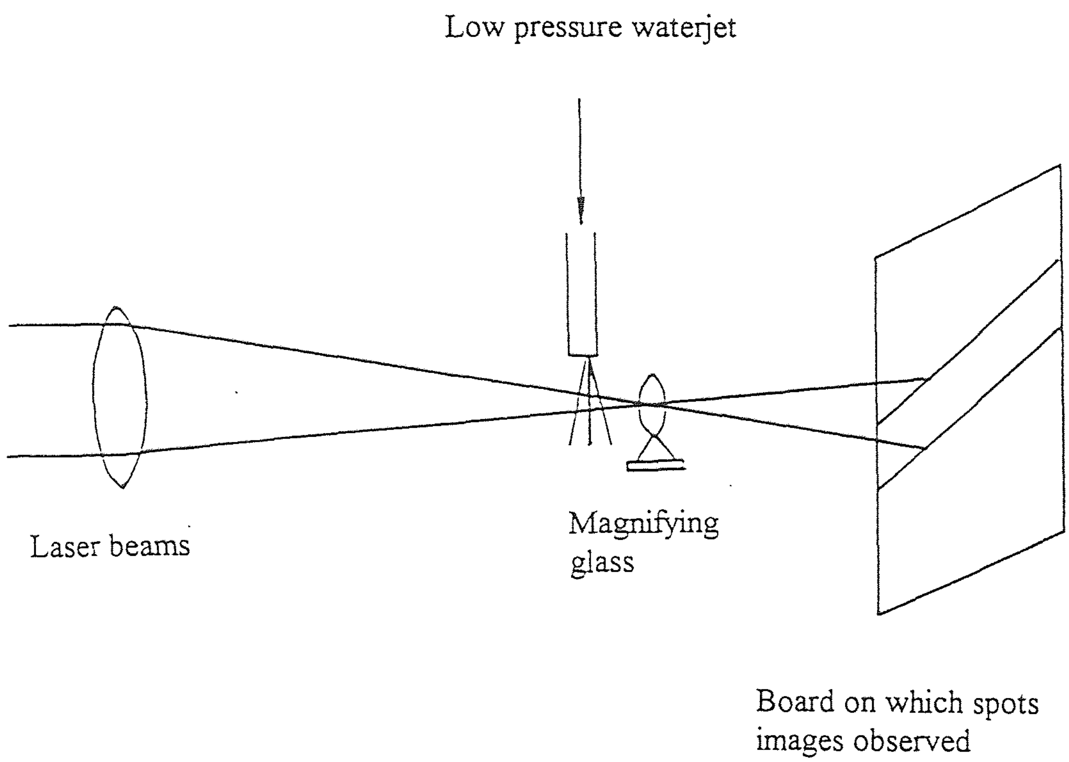

Figure 11 Checking the jet alignment with focusing spots

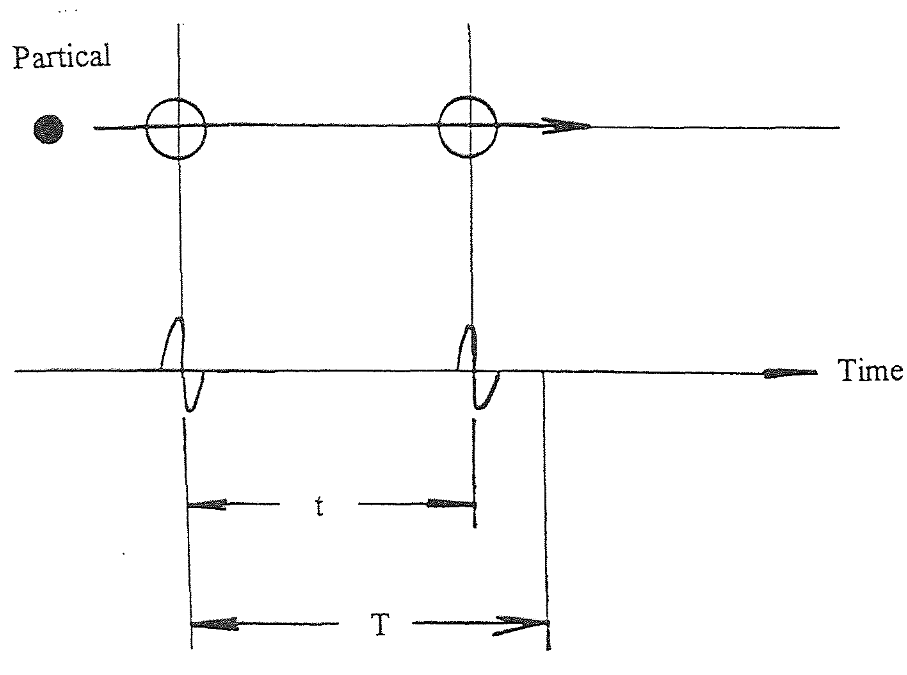

Figure 12 Pulse generation due to single particle

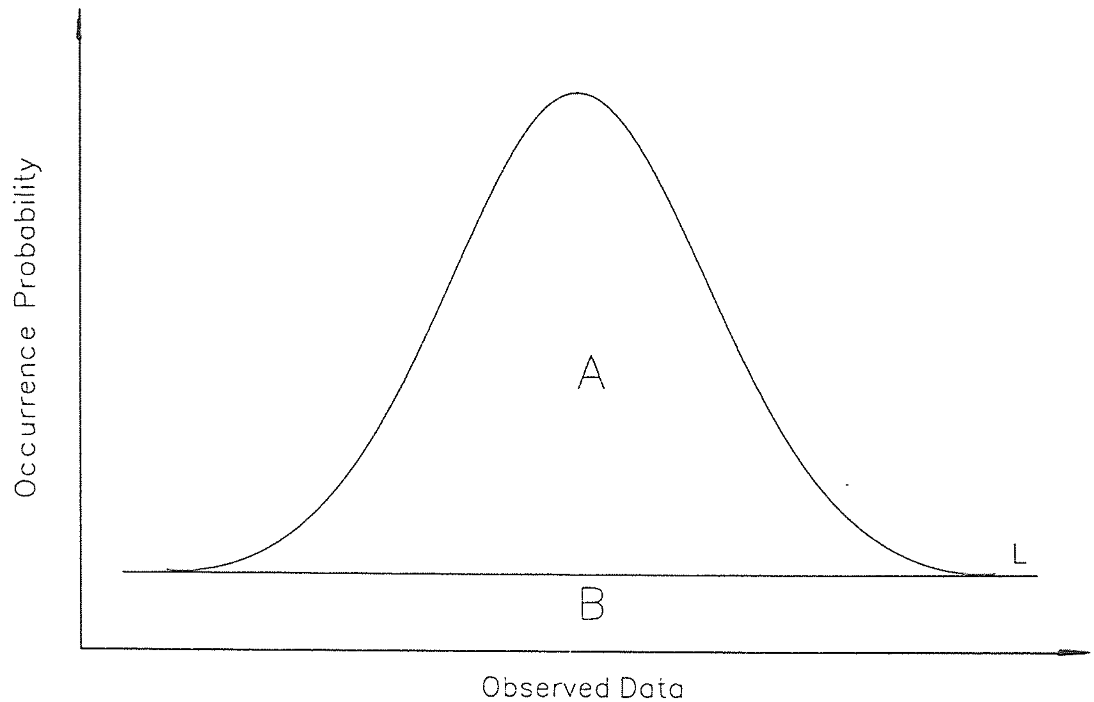

Figure 13 Occurrence probability distribution of observed data

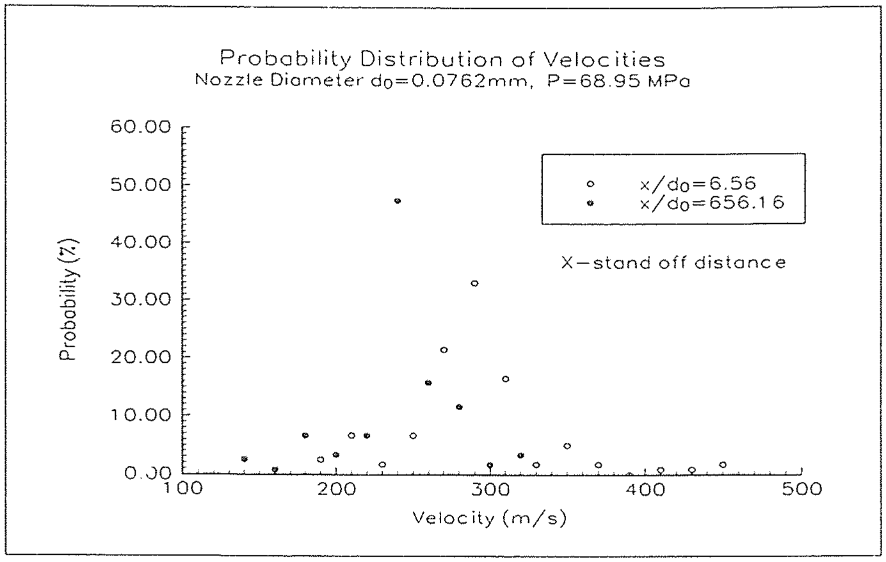

Figure 14 Probability distribution of axial velocities for nozzle diameter of 0.0762 mm under pressure of 68.95 MPa

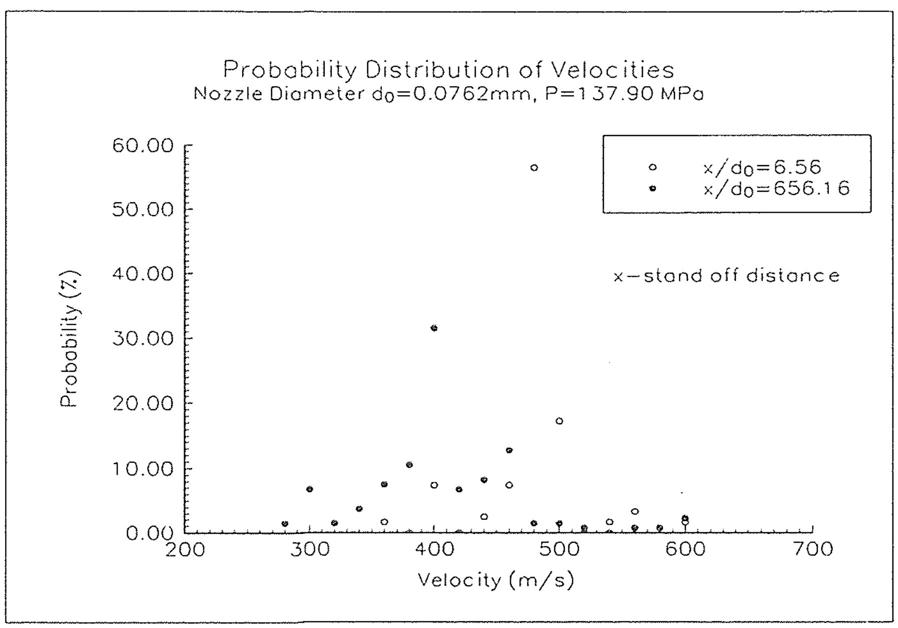

Figure 15 Probability distribution of axial velocities for nozzle diameter of 0.0762 mm under pressure of 137.90 MPa

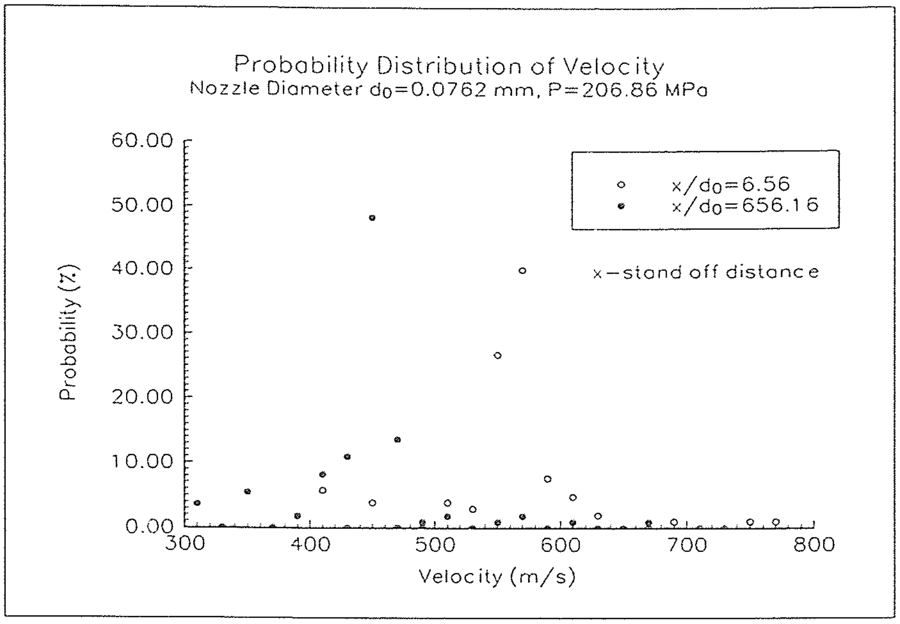

Figure 16 Probability distribution of axial velocities for nozzle diameter of 0.0762 mm under pressure of 206.86 MPa

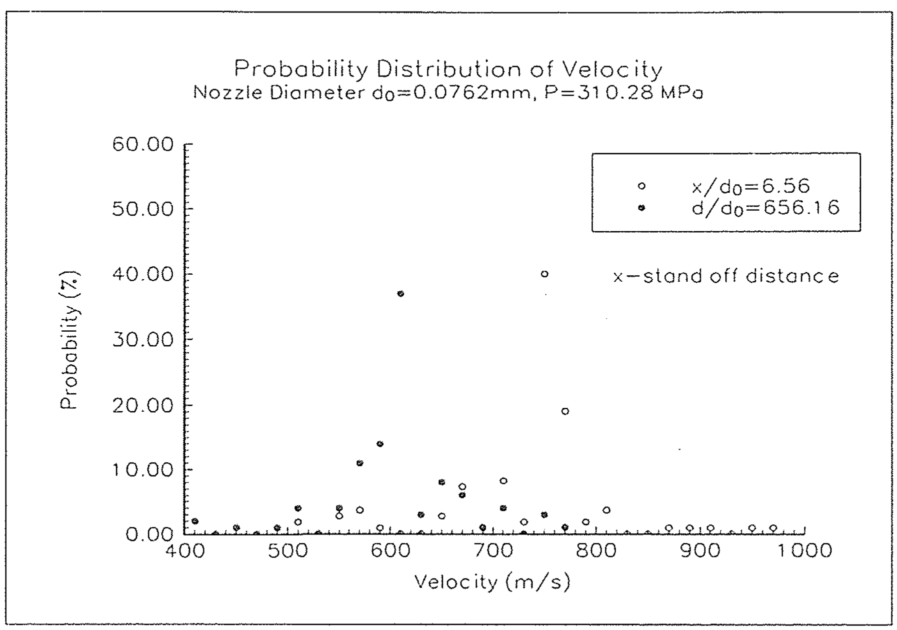

Figure 17 Probability distribution of axial velocities for nozzle diameter of 0.0762 mm under pressure of 310.28 MPa

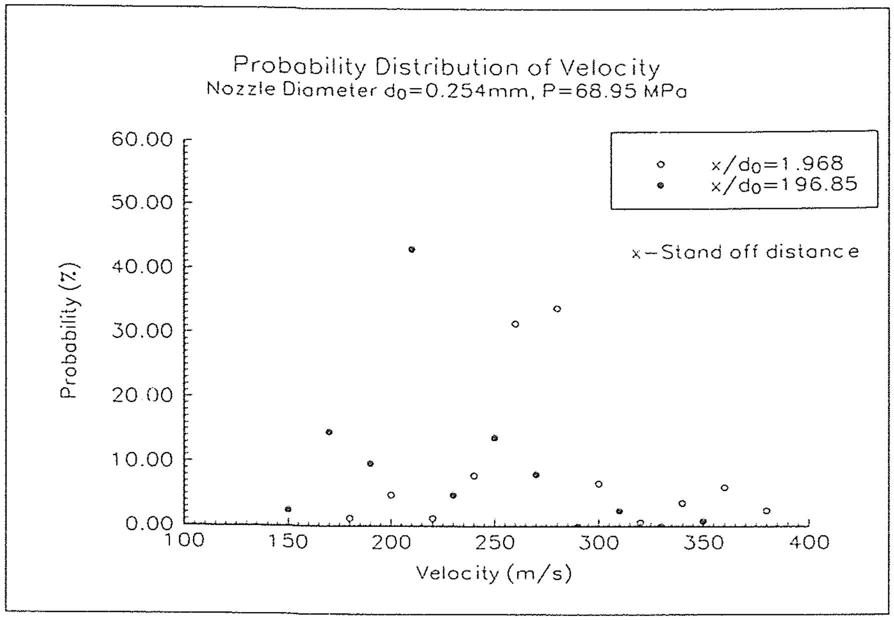

Figure 18 Probability distribution of axial velocities for nozzle diameter of 0.254 mm under pressure of 68.95 MPa

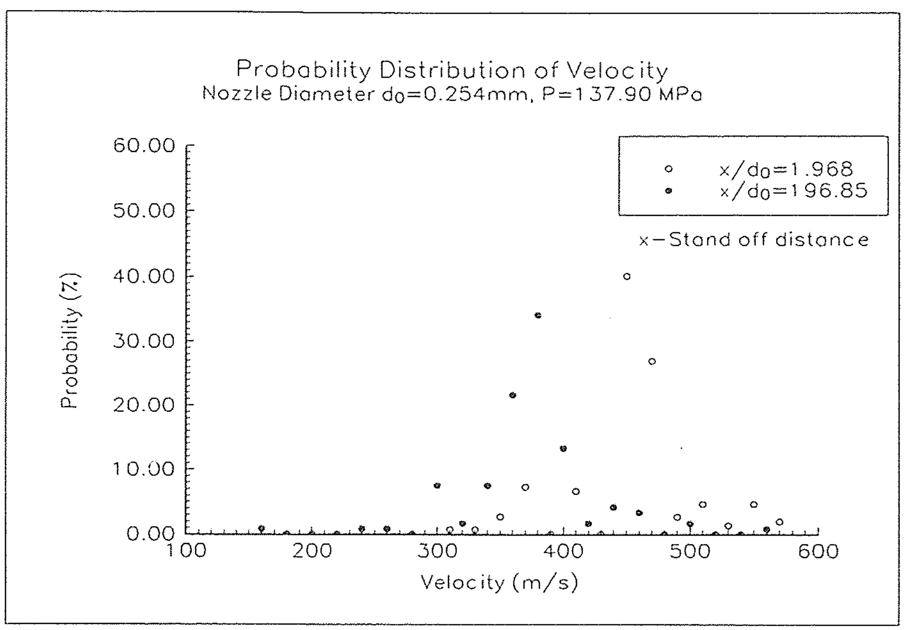

Figure 19 Probability distribution of axial velocities for nozzle diameter of 0.254 mm under pressure of 137.90 MPa

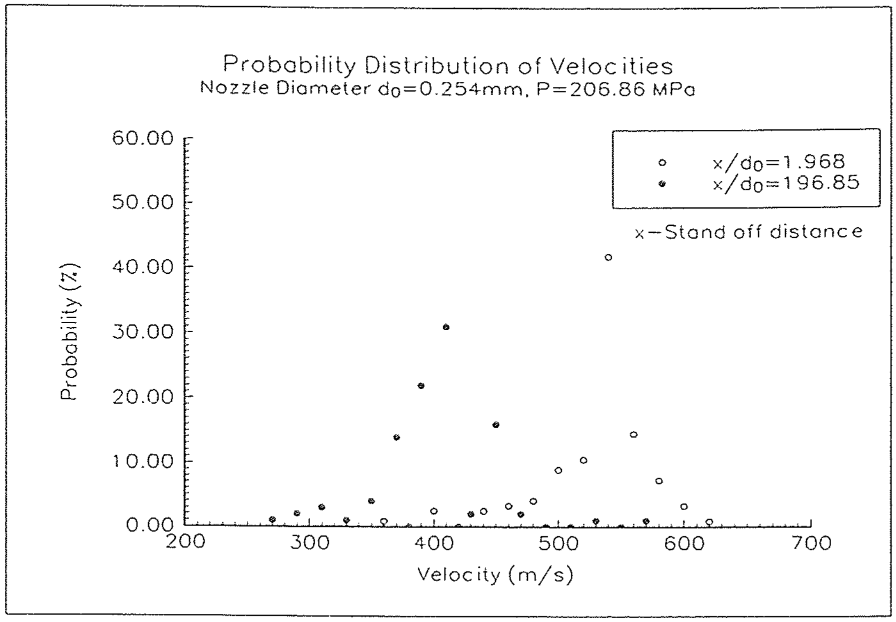

Figure 20 Probability distribution of axial velocities for nozzle diameter of 0.254 mm under pressure of 206.86 MPa

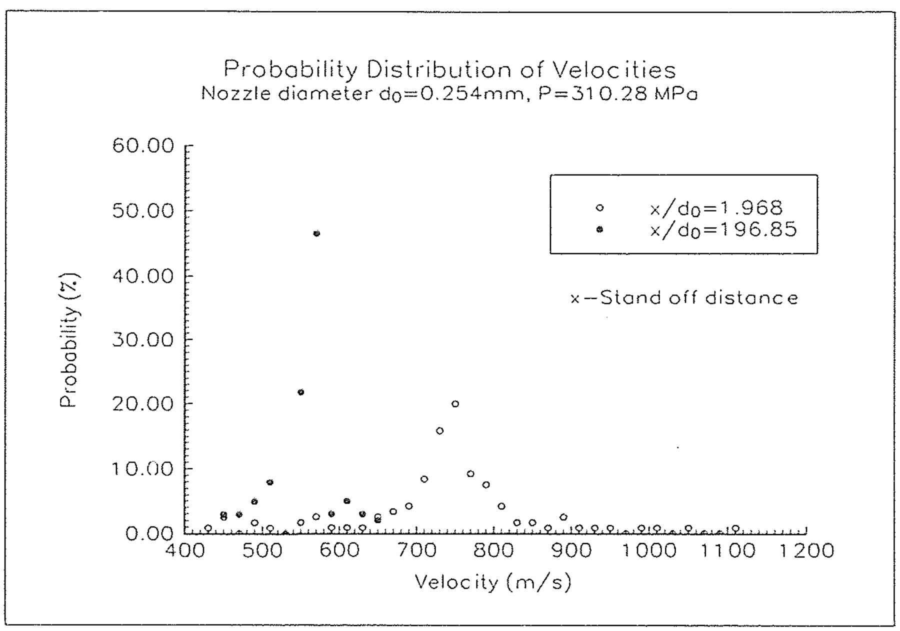

Figure 21 Probability distribution of axial velocities for nozzle diameter of 0.254 mm under pressure of 310.28 MPa

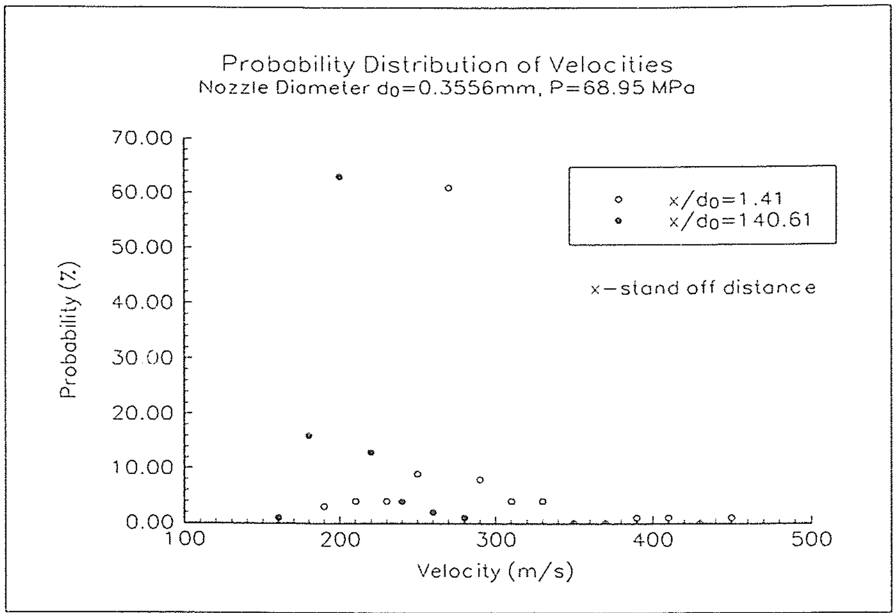

Figure 22 Probability distribution of axial velocities for nozzle diameter of 0.3556 mm under pressure of 68.95 MPa

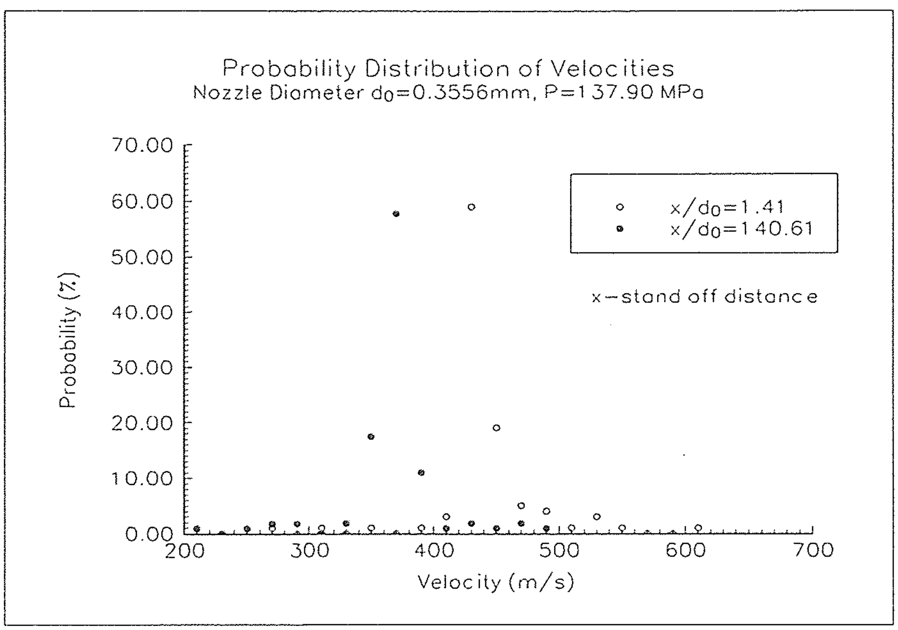

Figure 23 Probability distribution of axial velocities for nozzle diameter of 0.3556 mm under pressure of 137.90 MPa

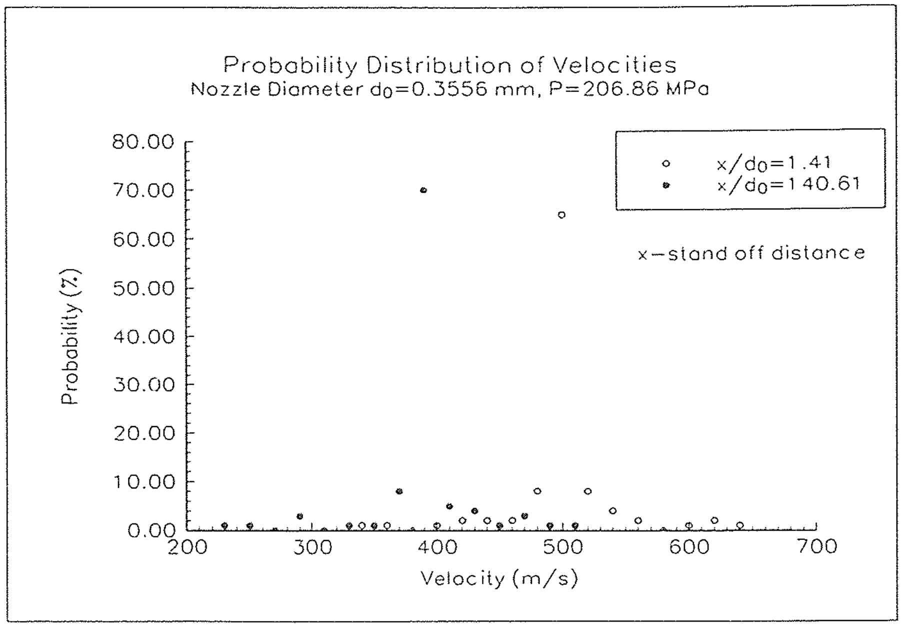

Figure 24 Probability distribution of axial velocities for nozzle diameter of 0.3556 mm under pressure of 206.86 MPa

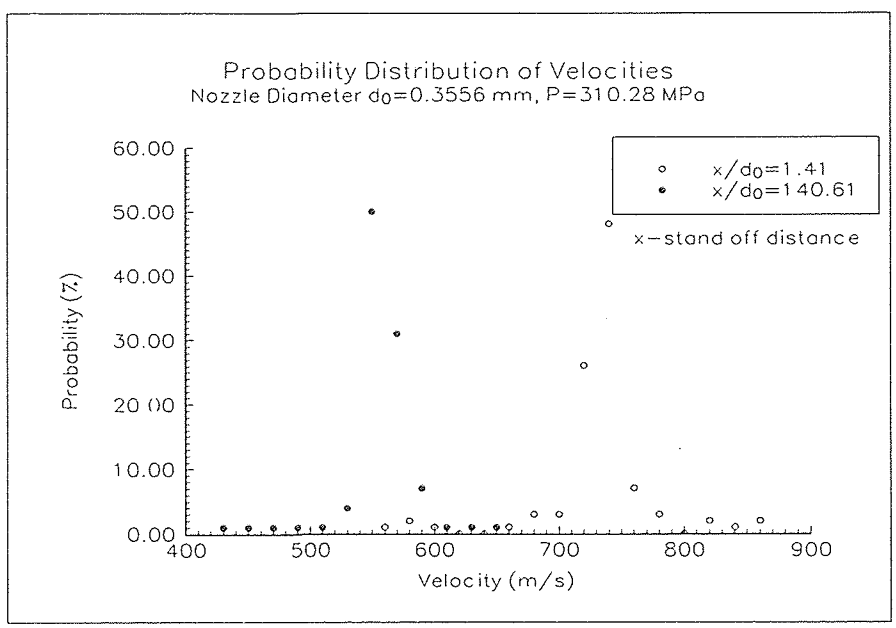

Figure 25 Probability distribution of axial velocities for nozzle diameter of 0.3556 mm under pressure of 310.28 MPa

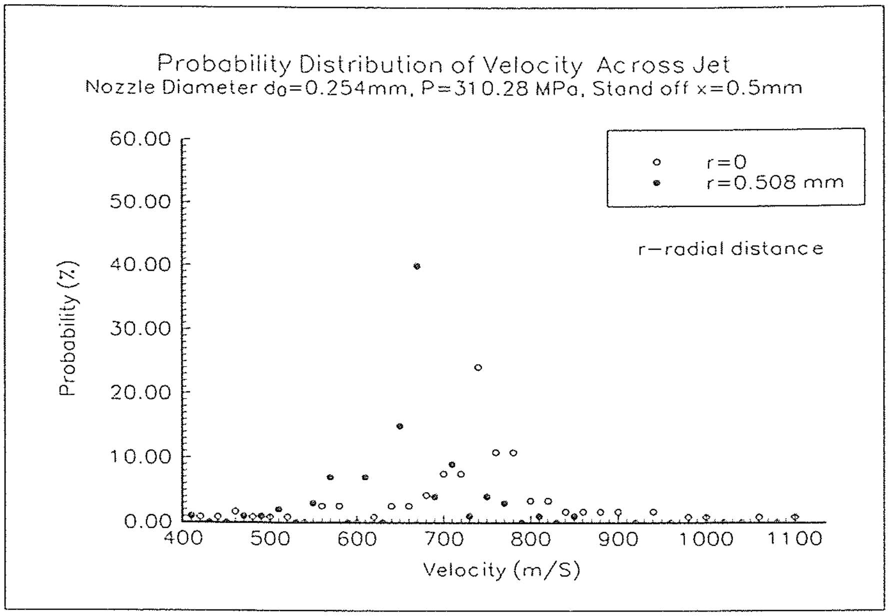

Figure 26 Probability distribution of velocities across jet for nozzle diameter of 0.254mm at stand off distance of 0.5 mm

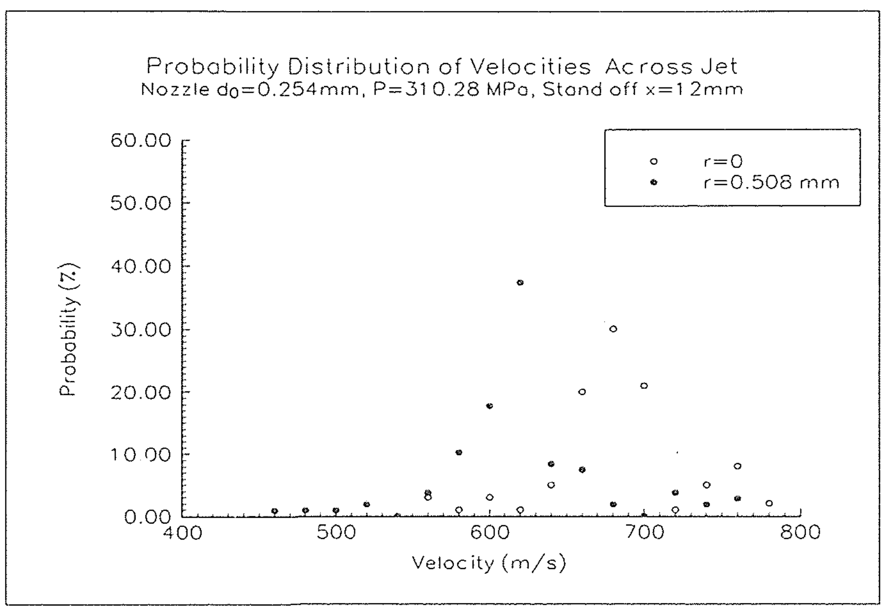

Figure 27 Probability distribution of velocities across jet for nozzle diameter of 0.254mm at stand off distance of 12 mm

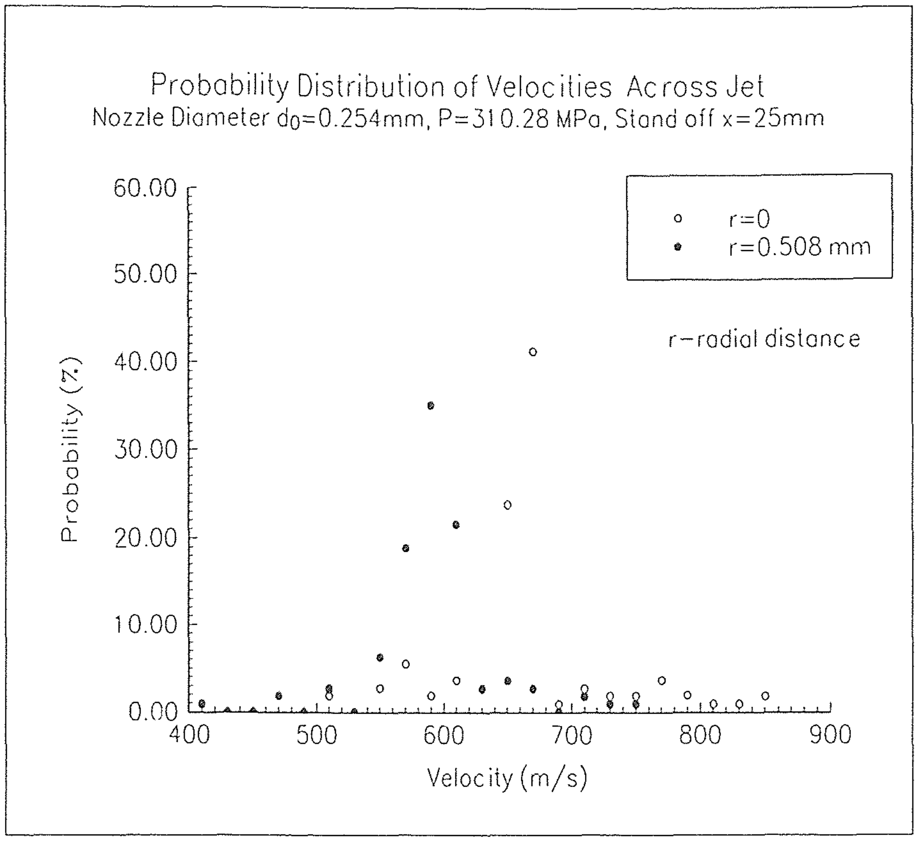

Figure 28 Probability distribution of velocities across jet for nozzle diameter of 0.254mm at stand off distance of 25 mm

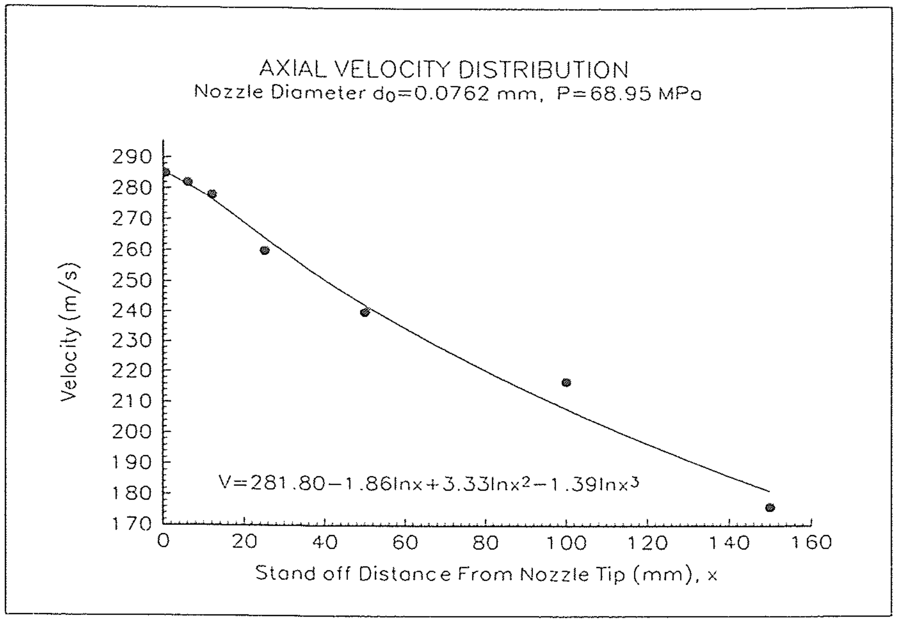

Figure 29 Axial velocity distribution for nozzle diameter of 0.0762 mm under pressure of 68.95 MPa

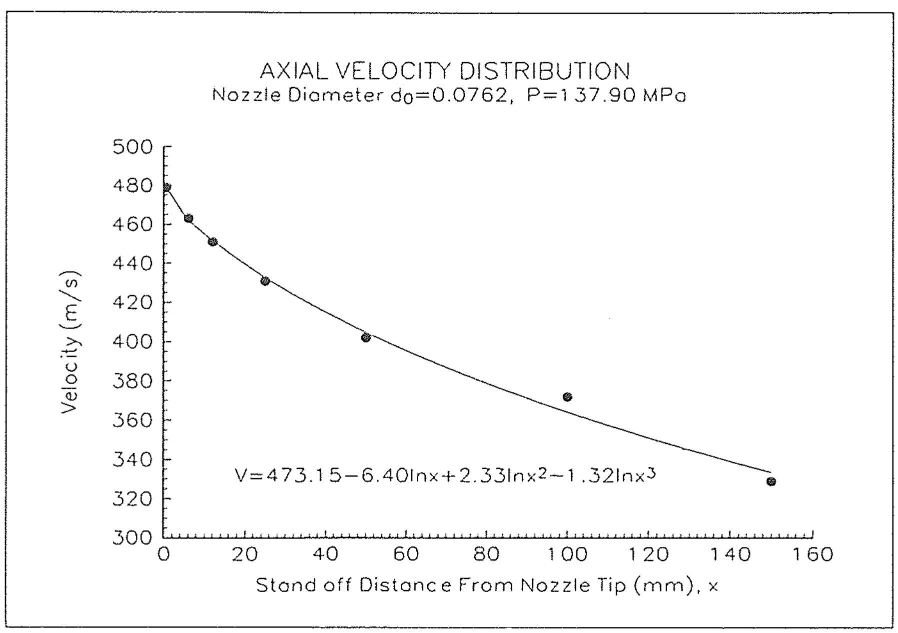

Figure 30 Axial velocity distribution for nozzle diameter of 0.076 mm under pressure of 137.90 MPa

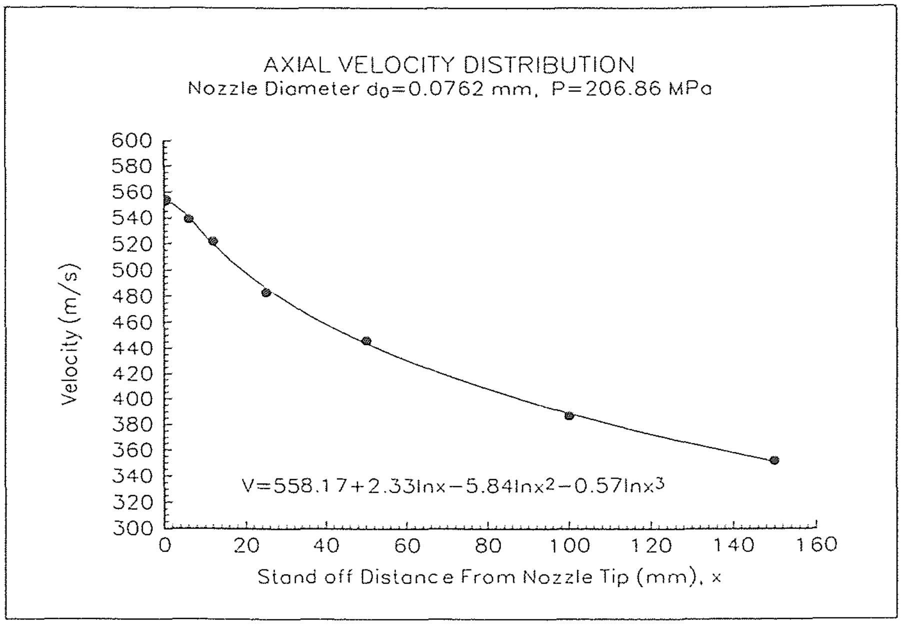

Figure 31 Axial velocity distribution for nozzle diameter of 0.0762 mm under pressure of 206.86 MPa

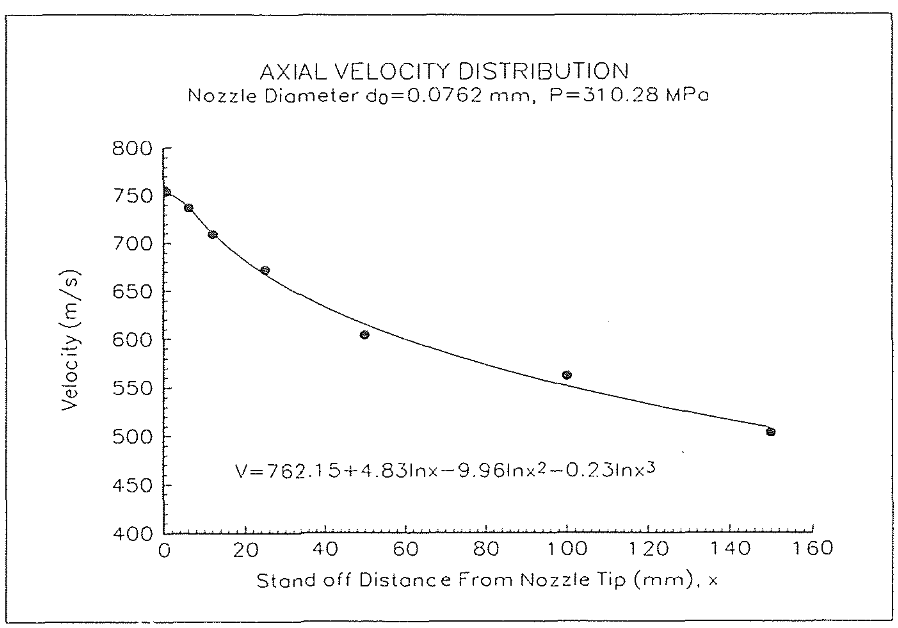

Figure 32 Axial velocity distribution for nozzle diameter of 0.0762 mm under pressure of 310.28 MPa

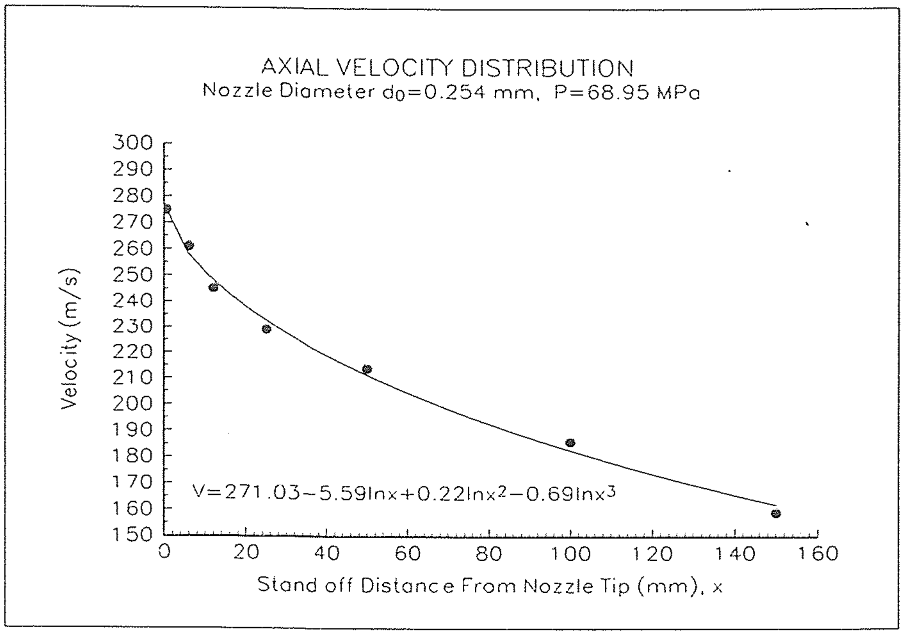

Figure 33 Axial velocity distribution for nozzle diameter of 0.254 mm under pressure of 68.95 MPa

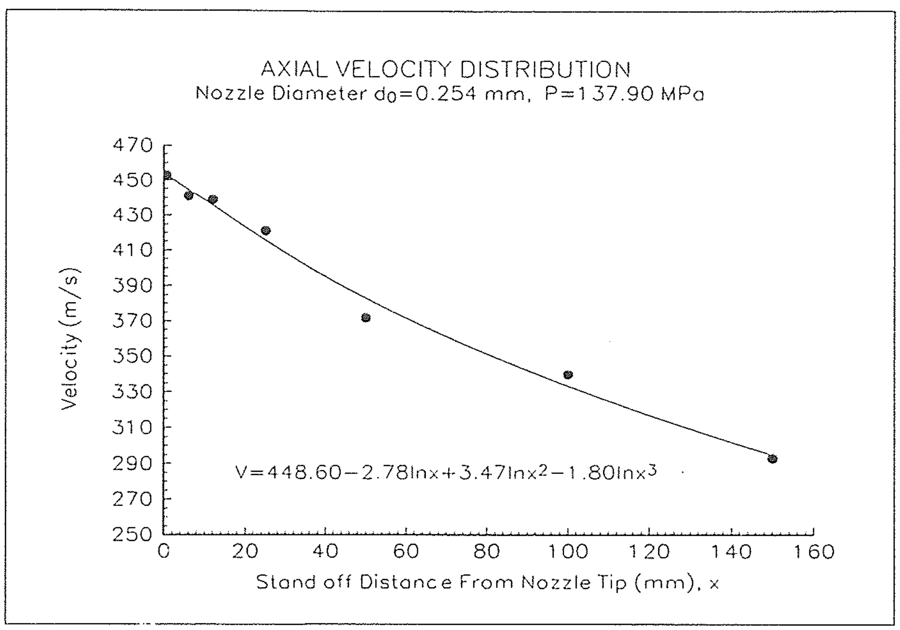

Figure 34 Axial velocity distribution for nozzle diameter of 0.254 mm under pressure of 137.90 MPa

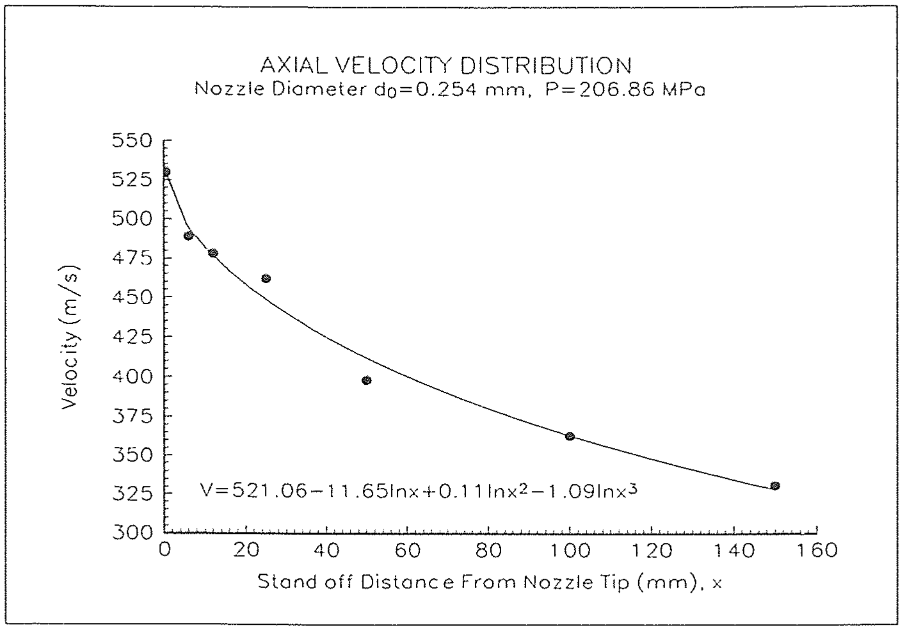

Figure 35 Axial velocity distribution for nozzle diameter of 0.254 mm under pressure of 206.86 MPa

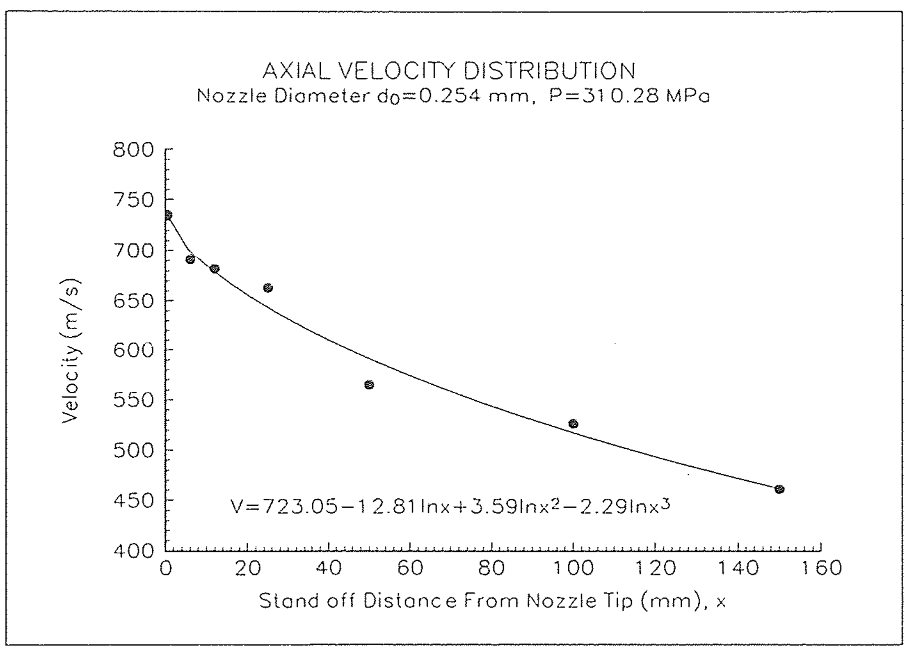

Figure 36 Axial velocity distribution for nozzle diameter of 0.254 mm under pressure of 310.28 MPa

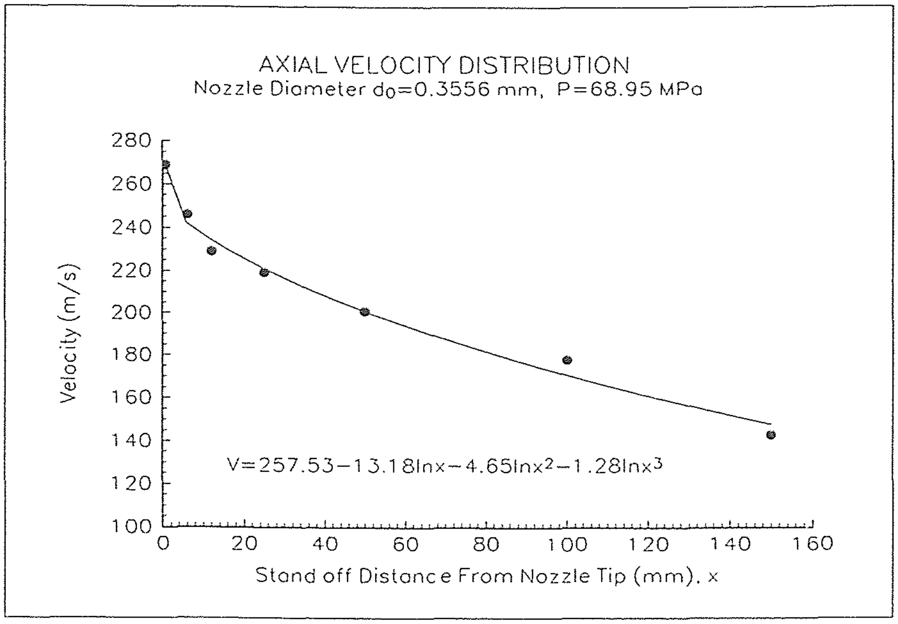

Figure 37 Axial velocity distribution for nozzle diameter of 0.3556 mm under pressure of 68.95 MPa

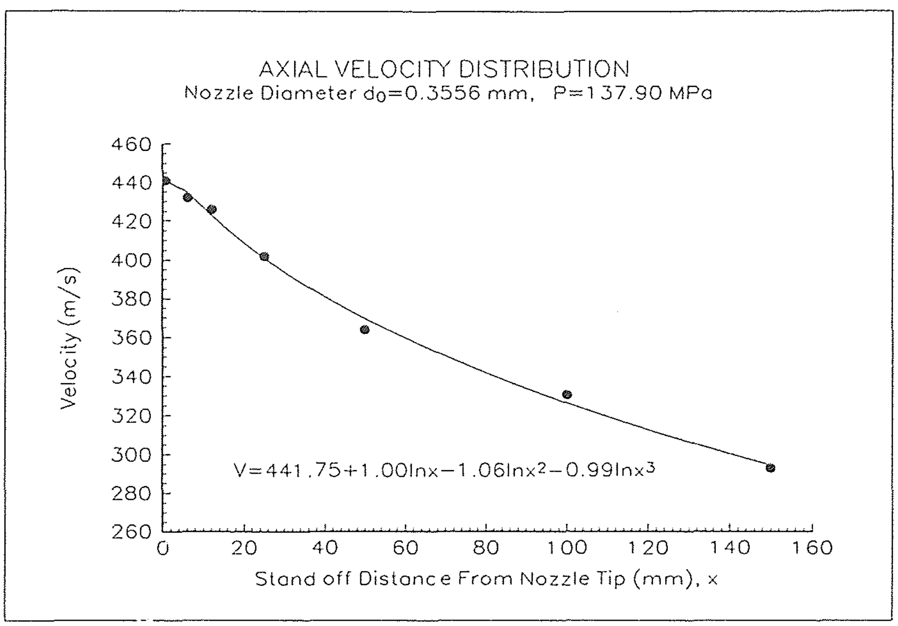

Figure 38 Axial velocity distribution for nozzle diameter of 0.3556 mm under pressure of 137.90 MPa

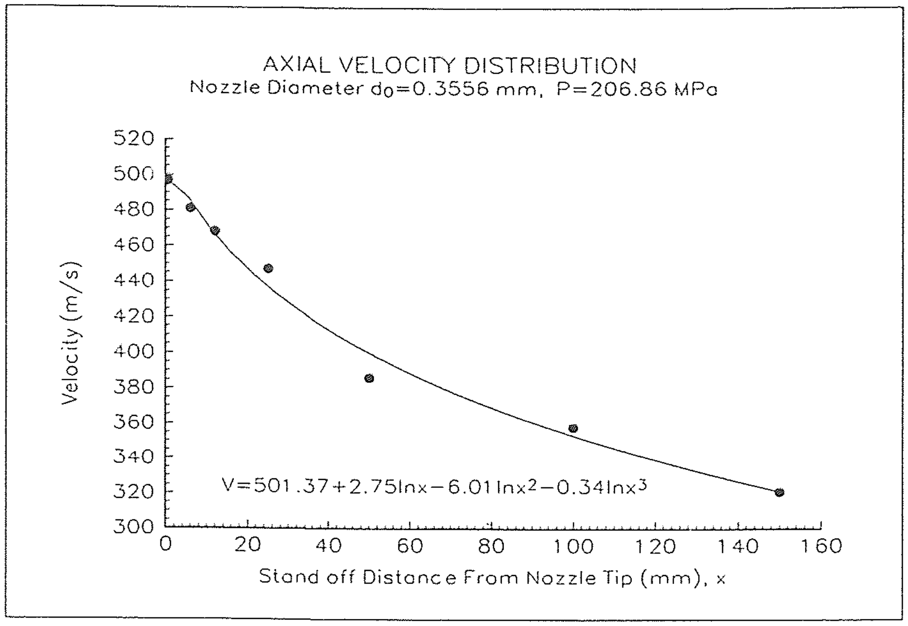

Figure 39 Axial velocity distribution for nozzle diameter of 0.3556 mm under pressure of 206.86 MPa

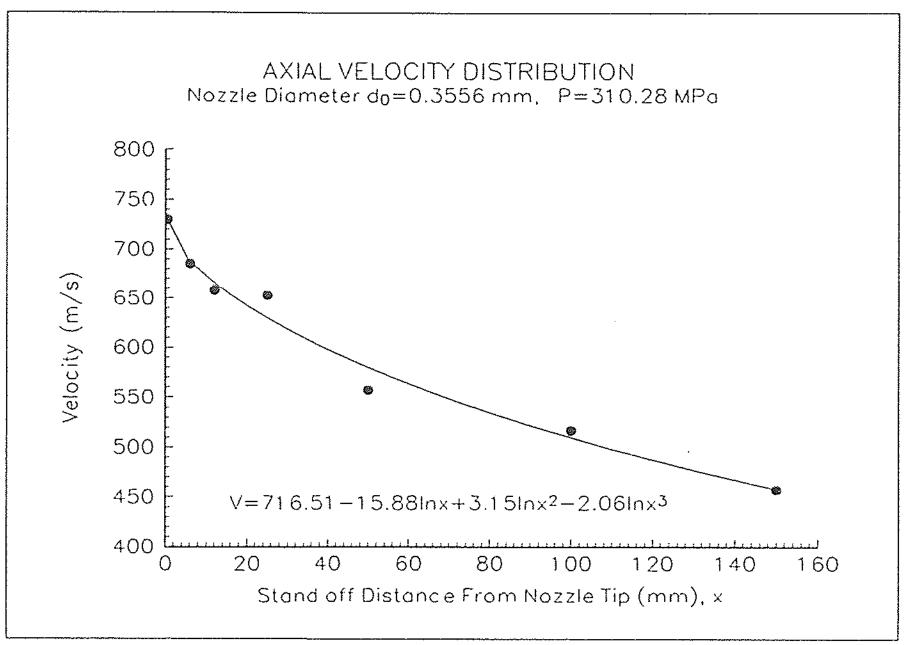

Figure 40 Axial velocity distribution for nozzle diameter of 0.3556 mm under pressure of 310.28 MPa

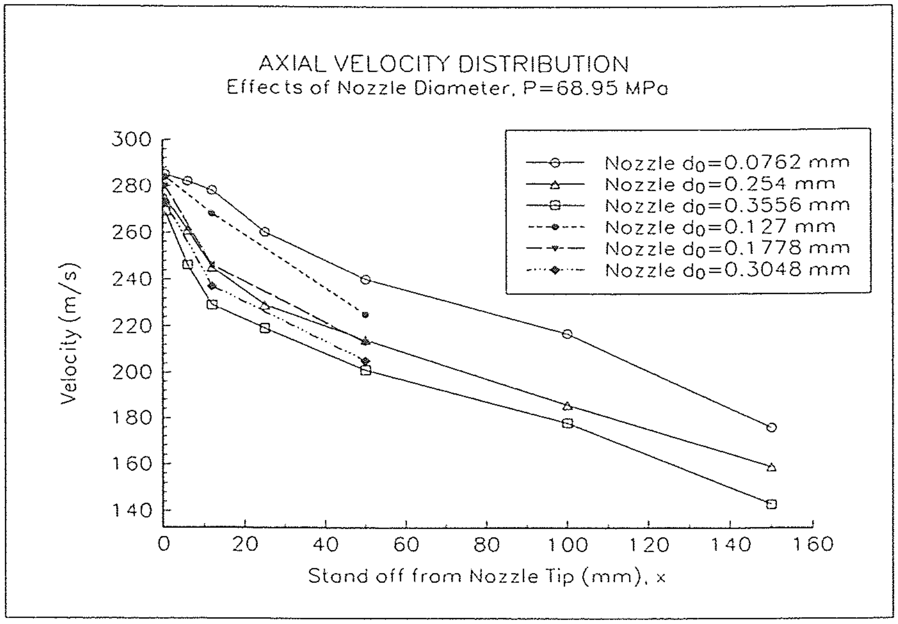

Figure 41 Axial velocity distribution for different nozzle diameter under pressure of 68.95 MPa

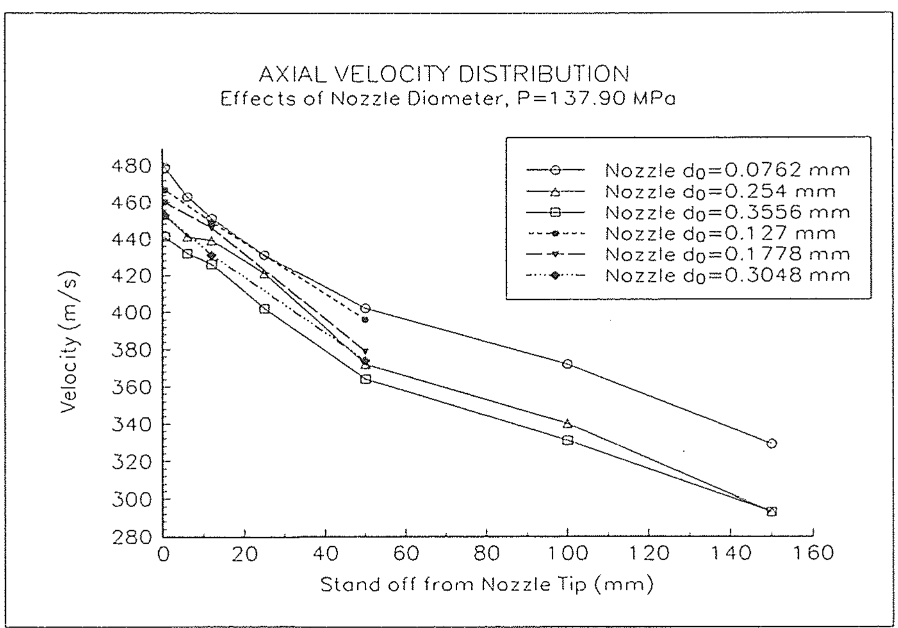

Figure 42 Axial velocity distribution for different nozzle diameter under pressure of 137.90 MPa

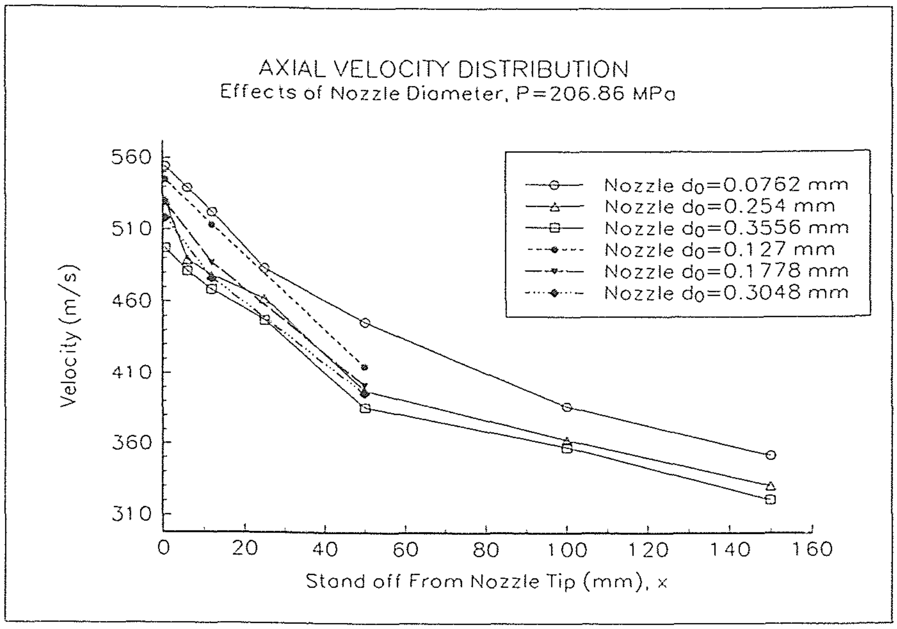

Figure 43 Axial velocity distribution for different nozzle diameter under pressure of 206.86 MPa

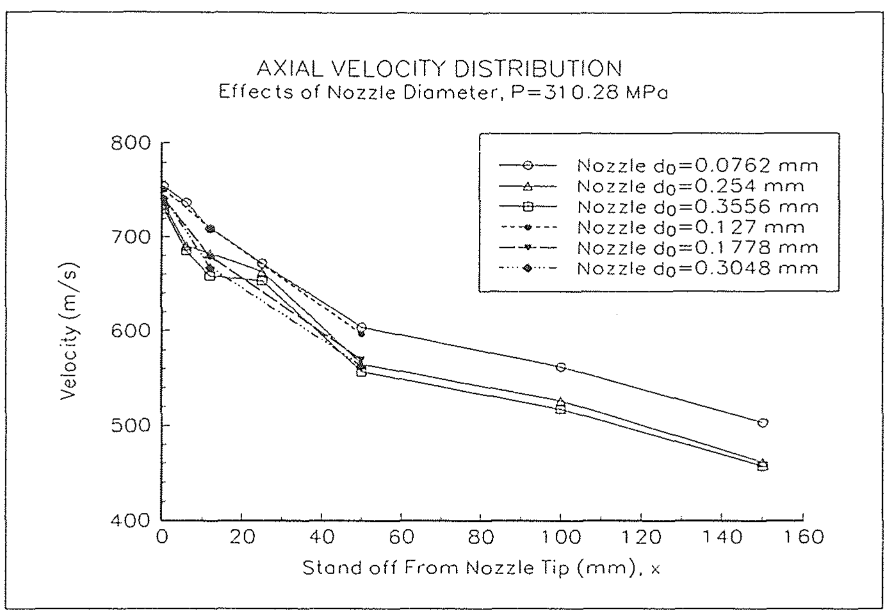

Figure 44 Axial velocity distribution for different nozzle diameter under pressure of 310.28 MPa

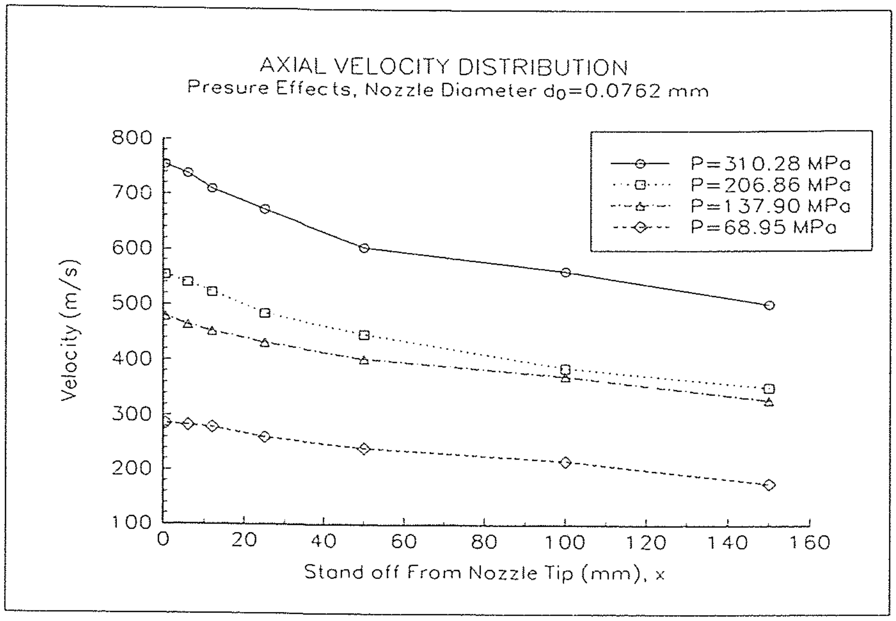

Figure 45 Axial velocity distribution for nozzle diameter of 0.762 mm under different pressures

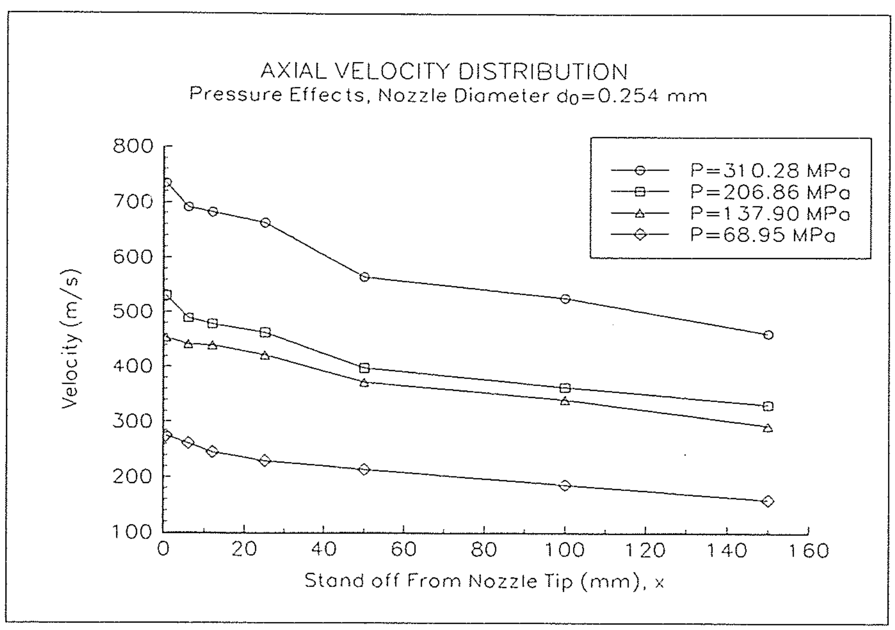

Figure 46 Axial velocity distribution for nozzle diameter of 0.254 mm under different pressures

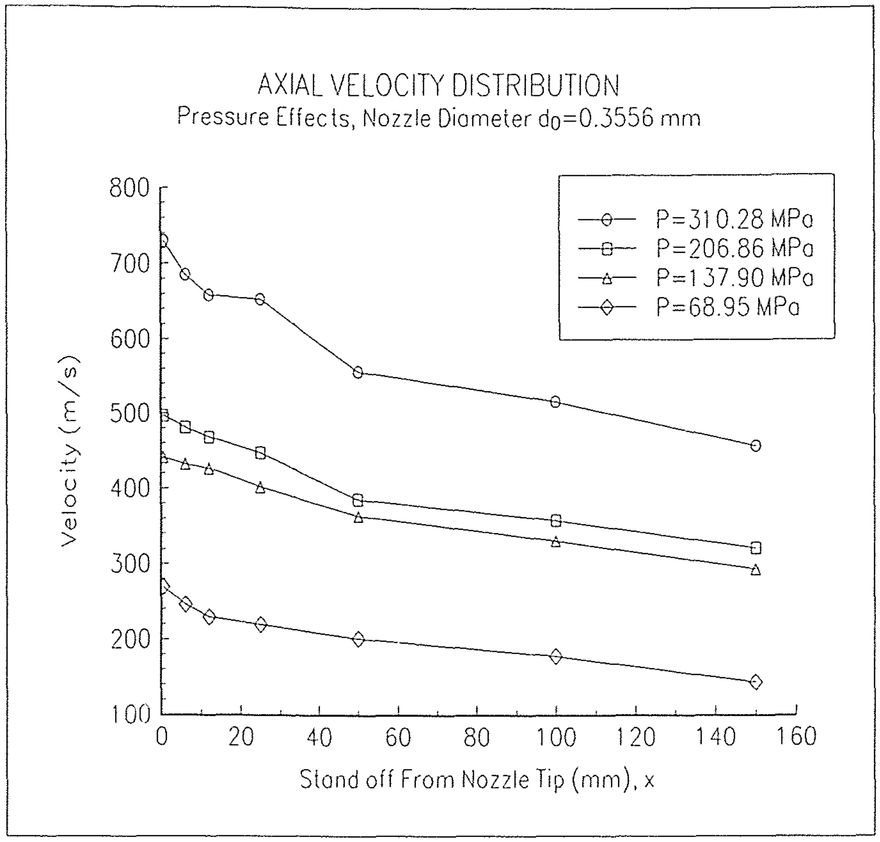

Figure 47 Axial velocity distribution for nozzle diameter of 0.3556 mm under different pressures

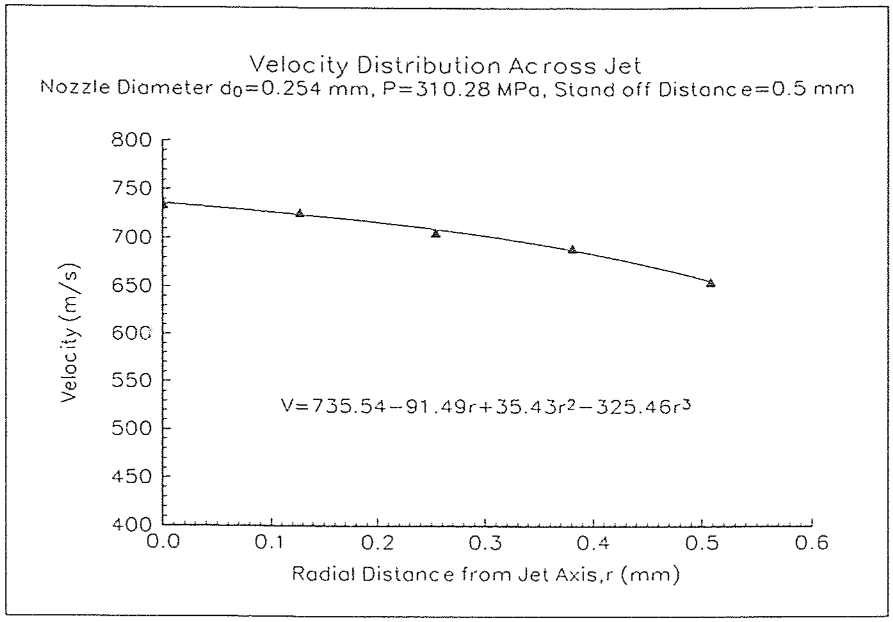

Figure 48 Velocity distribution across jet for nozzle diameter of 0.254 mm at stand off distance of 0.5 mm

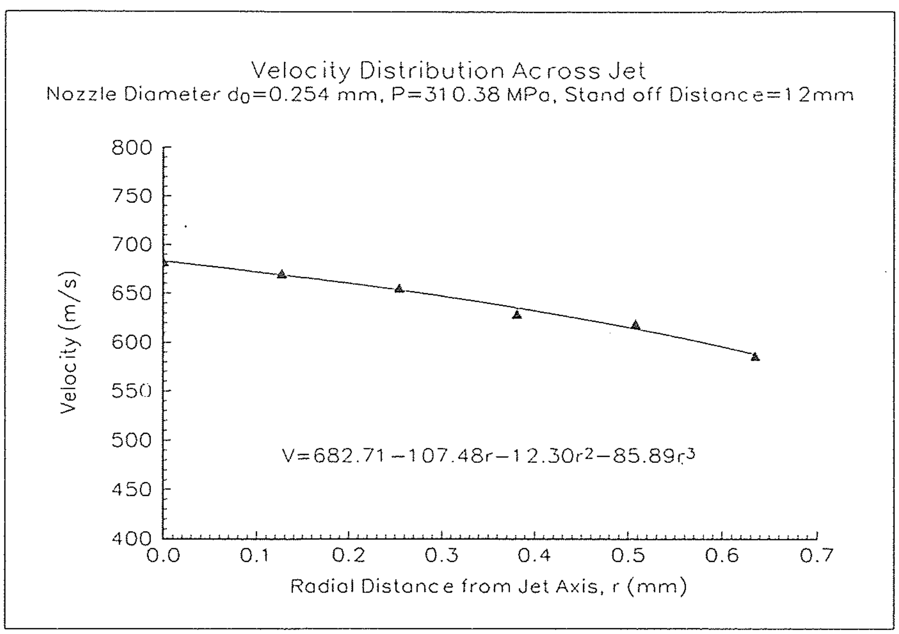

Figure 49 Velocity distribution across jet for nozzle diameter of 0.254 mm at stand off distance of 12 mm

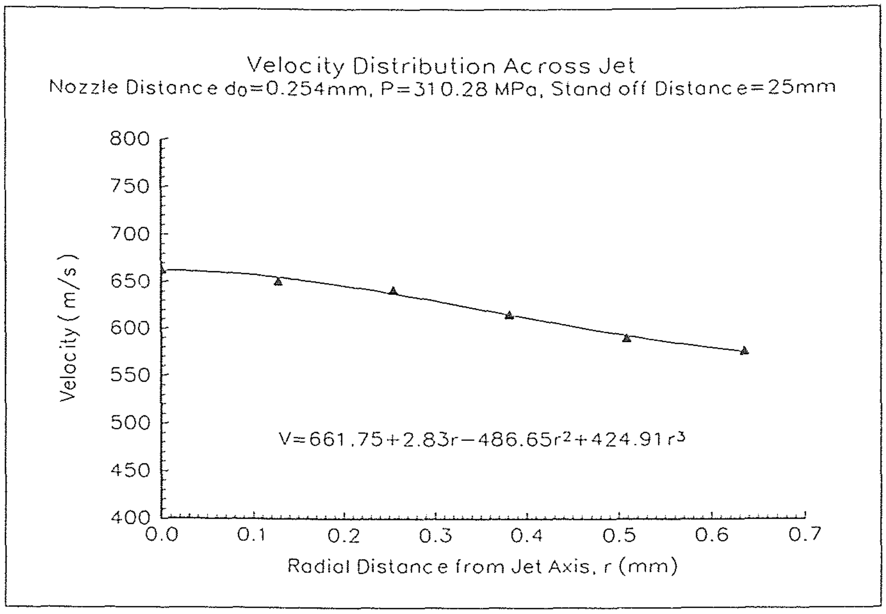

Figure 50 Velocity distribution across jet for nozzle diameter of 0.254 mm at stand off distance of 25 mm

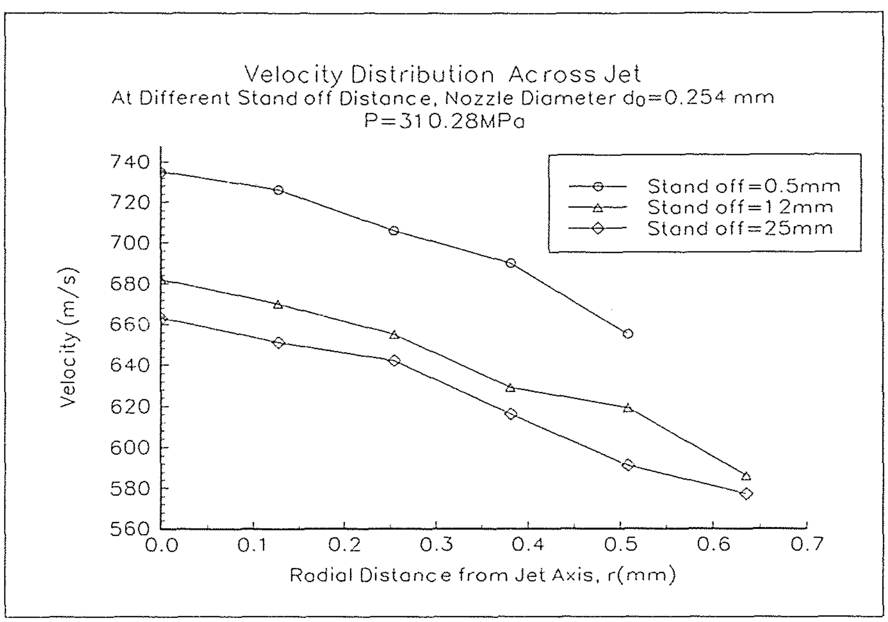

Figure 51 Velocity distribution across jet for nozzle diameter of 0.254 mm at different stand off distances

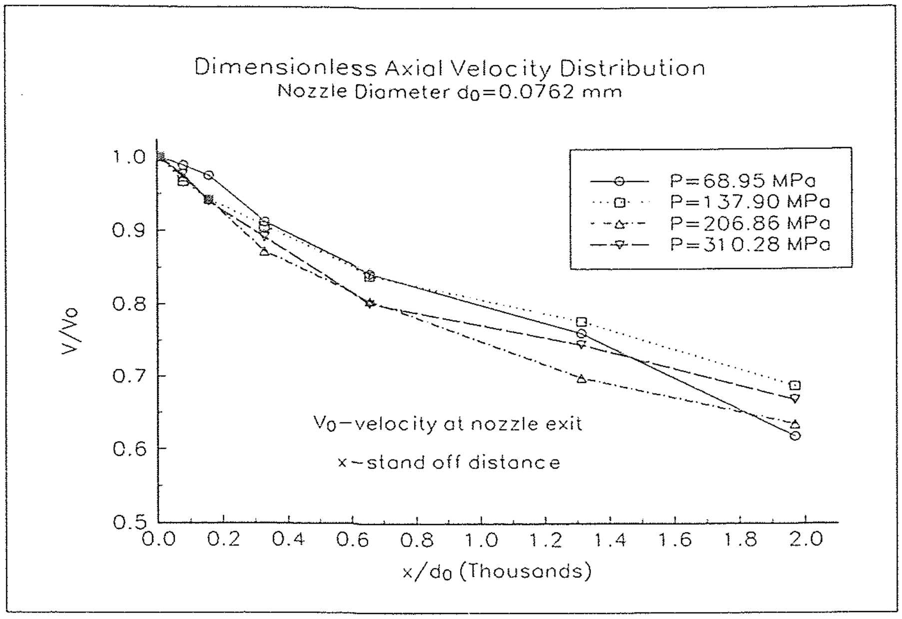

Figure 52 Dimensionless axial velocity distribution for nozzle diameter of 0.0762 mm under different pressures

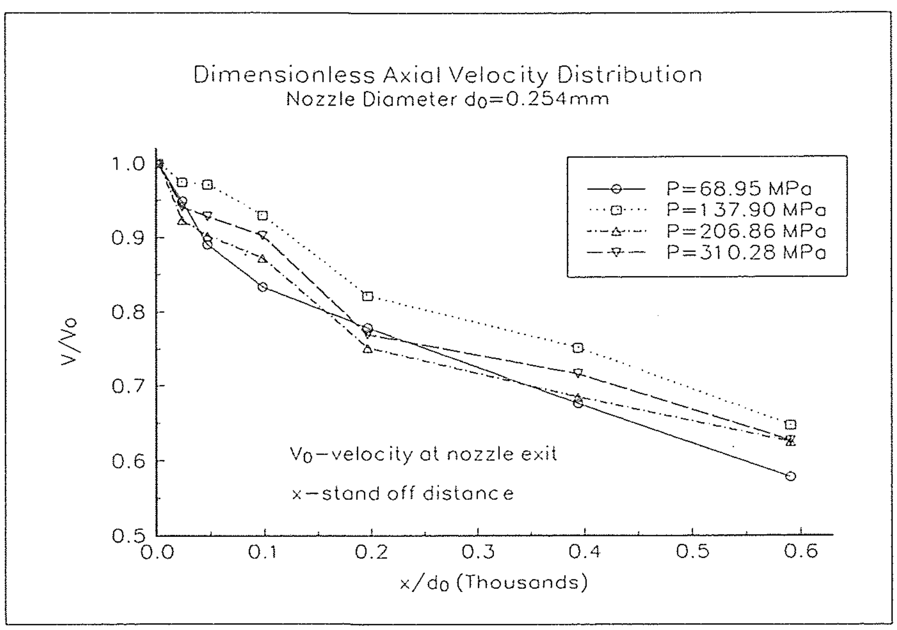

Figure 53 Dimensionless axial velocity distribution for nozzle diameter of 0.254 mm under different pressures

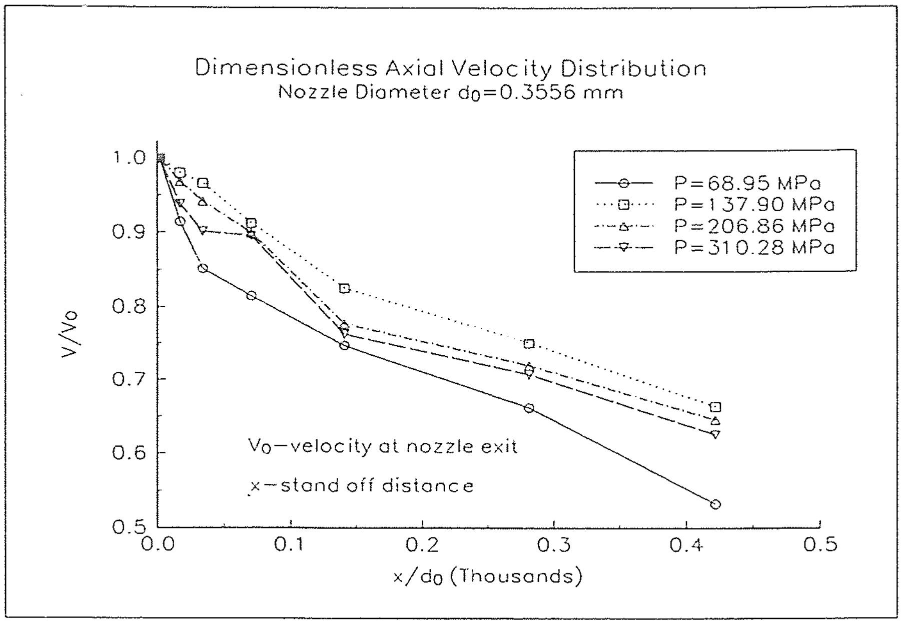

Figure 54 Dimensionless axial velocity distribution for nozzle diameter of 0.3556 mm under different pressures

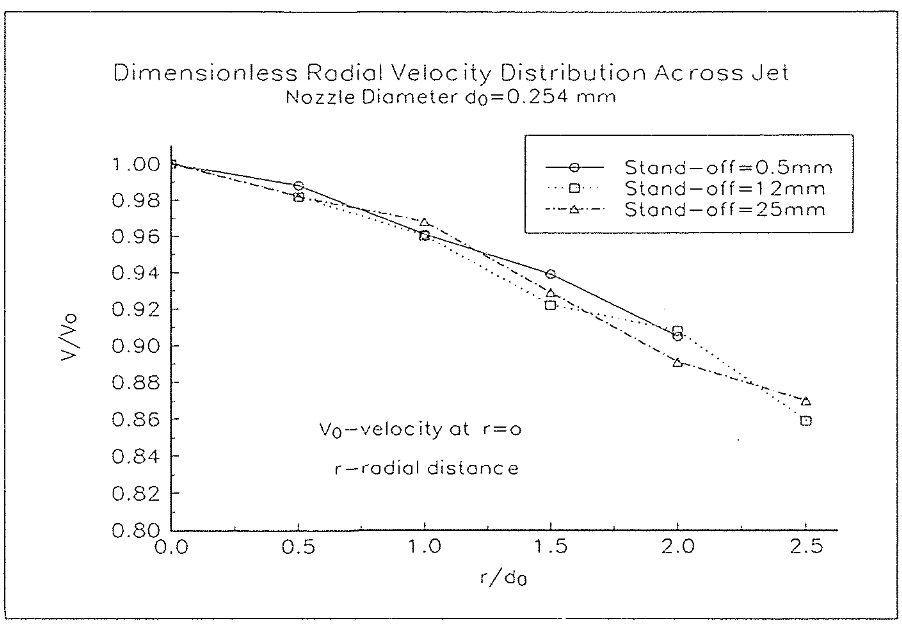

Figure 55 Dimensionless radial velocity distribution across jet for nozzle diameter of 0.254 mm at different stand off distances

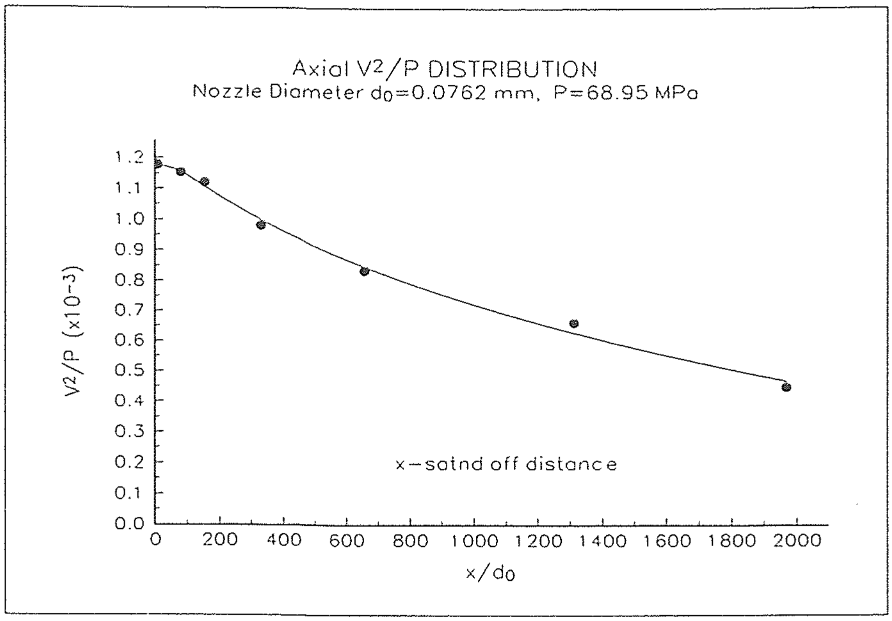

Figure 56 Axial V^2/P distribution for nozzle diameter of 0.0762 mm under pressure of 68.95 MPa

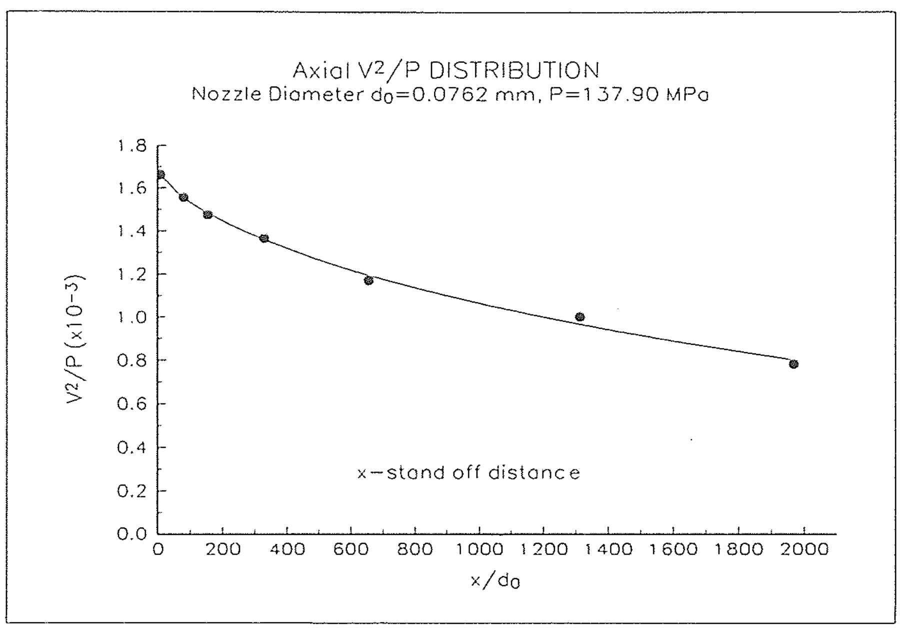

Figure 57 Axial V^2/P distribution for nozzle diameter of 0.0762 mm under pressure of 137.90 MPa

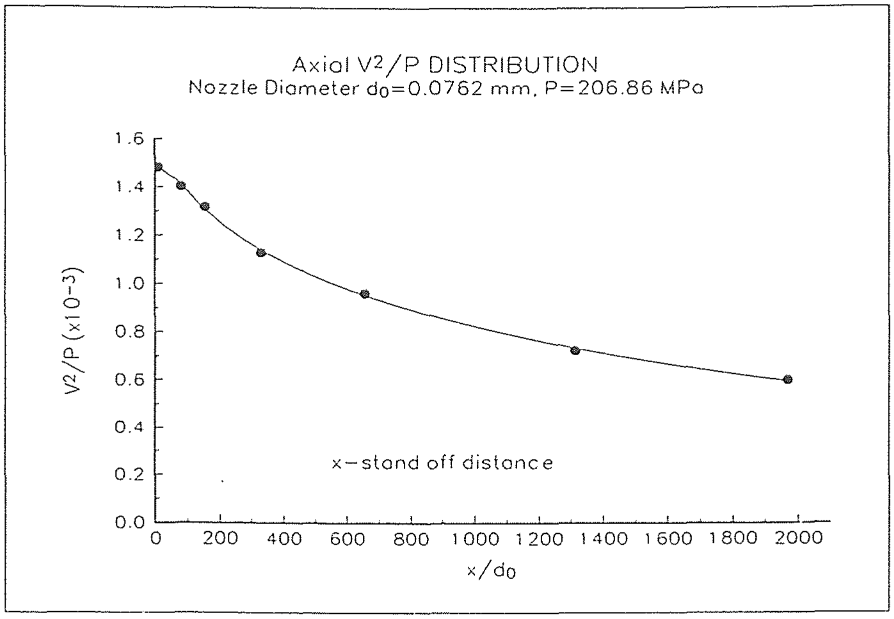

Figure 58 Axial V^2/P distribution for nozzle diameter of 0.0762 mm under pressure of 206.86 MPa

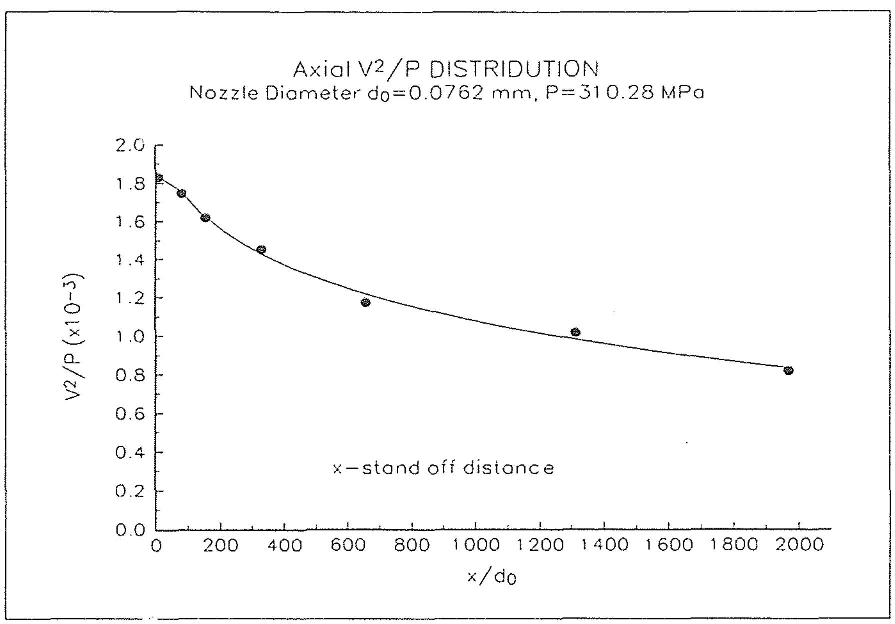

Figure 59 Axial V^2/P distribution for nozzle diameter of 0.0762 mm under pressure of 310.28 MPa

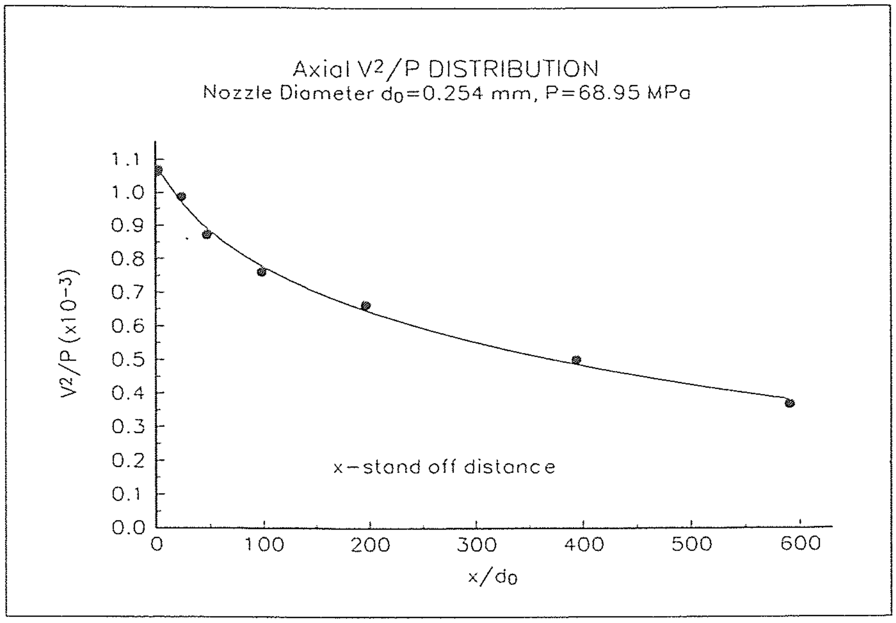

Figure 60 Axial V^2/P distribution for nozzle diameter of 0.254 mm under pressure of 68.95 MPa

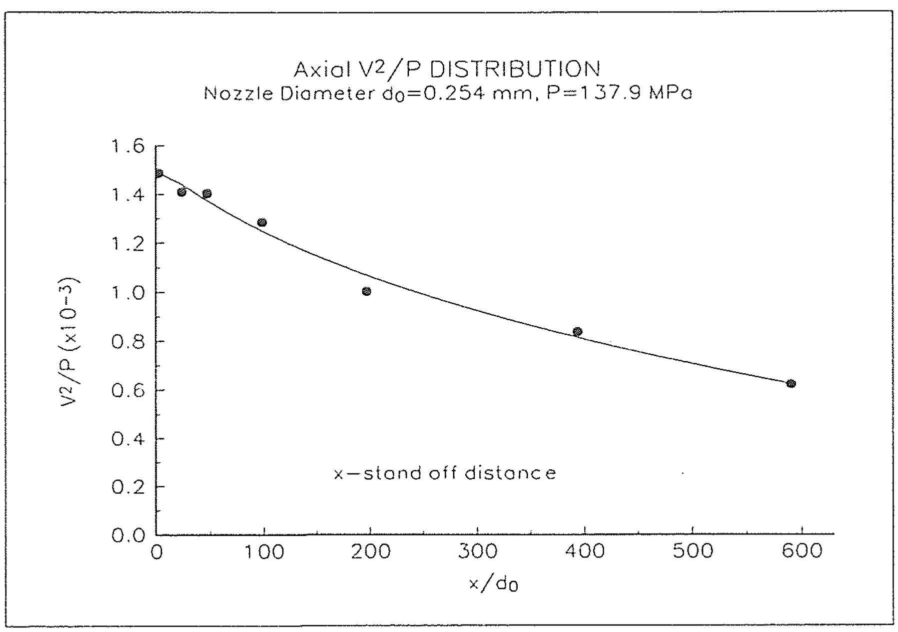

Figure 61 Axial V^2/P distribution for nozzle diameter of 0.254 mm under pressure of 137.90 MPa

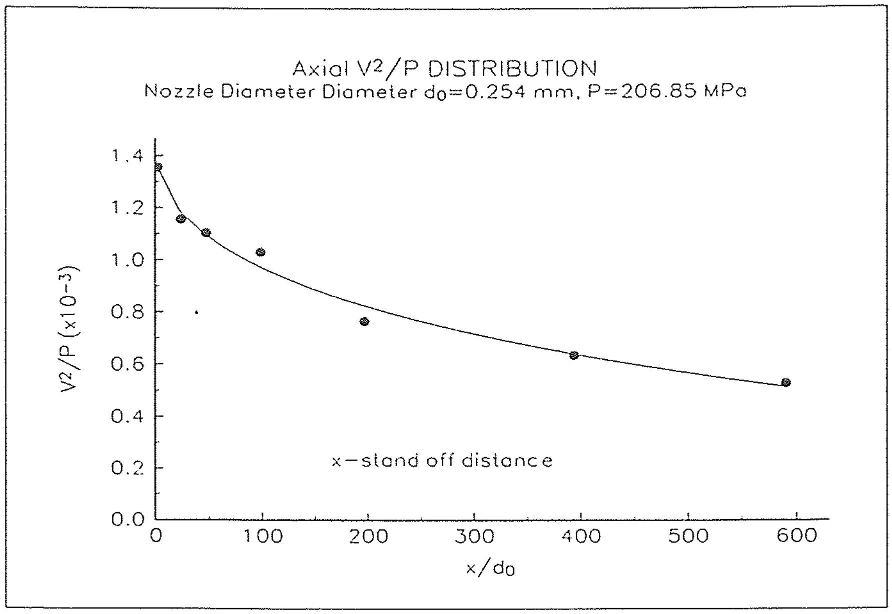

Figure 62 Axial V^2/P distribution for nozzle diameter of 0.254 mm under pressure of 206.85 MPa

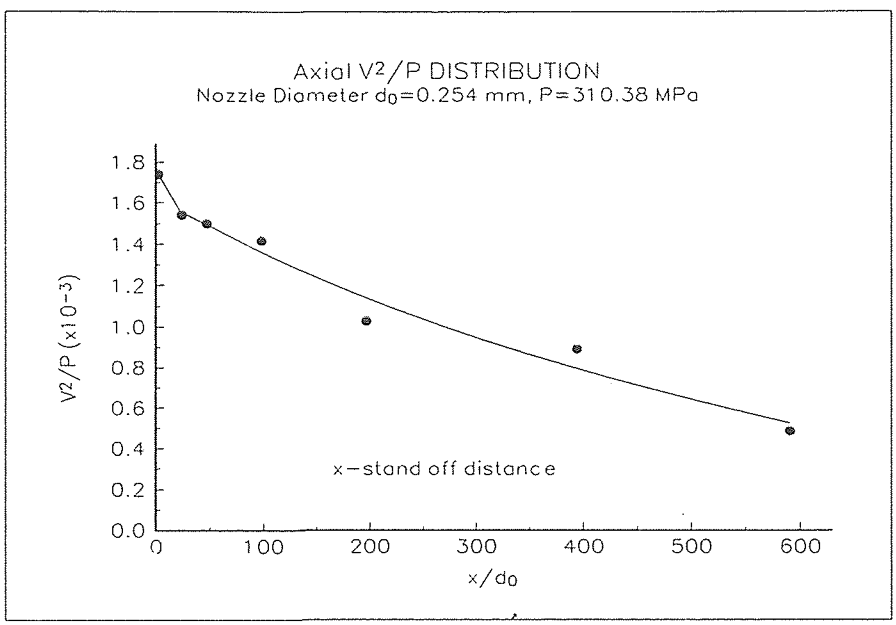

Figure 63 Axial V^2/P distribution for nozzle diameter of 0.254 mm under pressure of 310.28 MPa

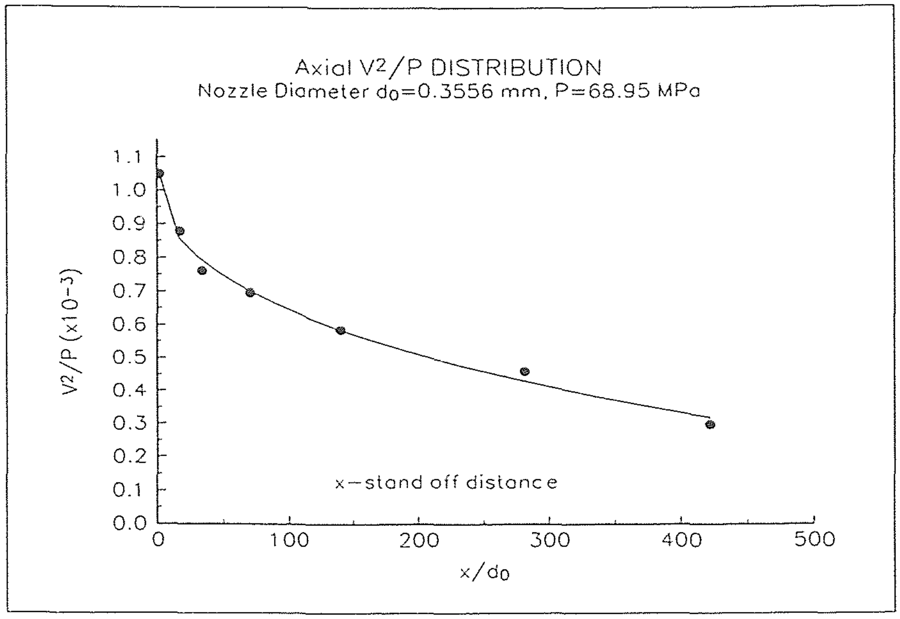

Figure 64 Axial V^2/P distribution for nozzle diameter of 0.3556 mm under pressure of 68.95 MPa

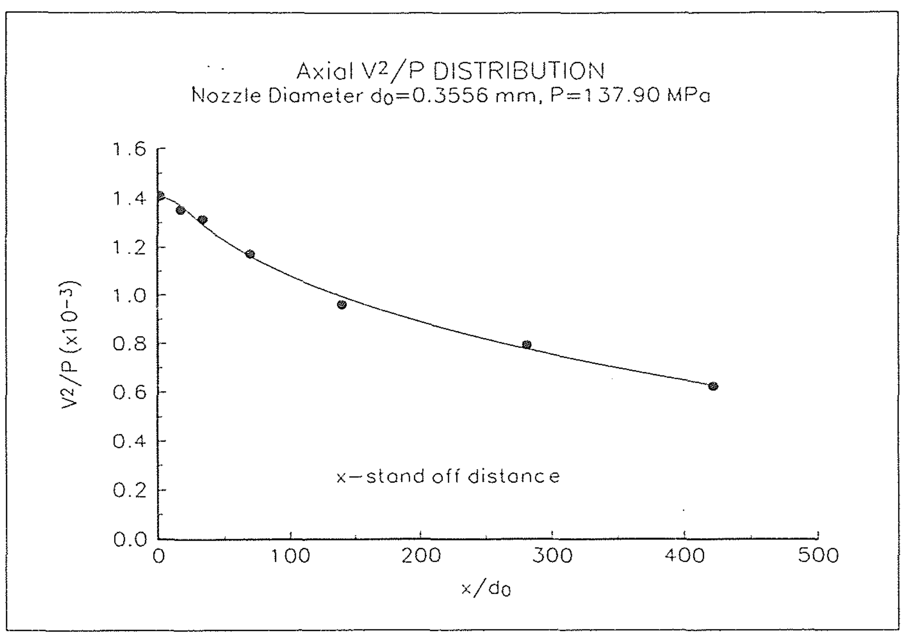

Figure 65 Axial V^2/P distribution for nozzle diameter of 0.3556 mm under pressure of 137.90 MPa

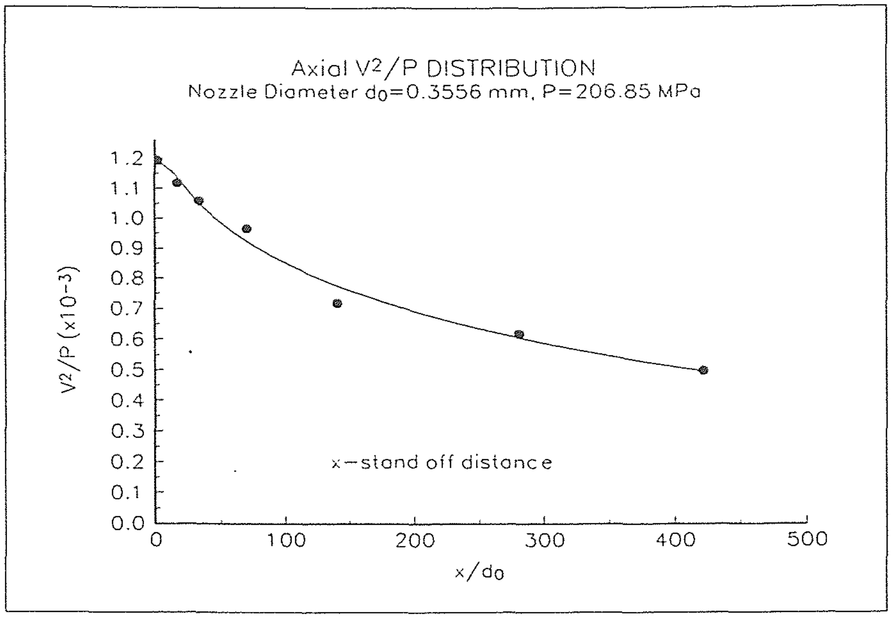

Figure 66 Axial V^2/P distribution for nozzle diameter of 0.3556 mm under pressure of 206.85 MPa

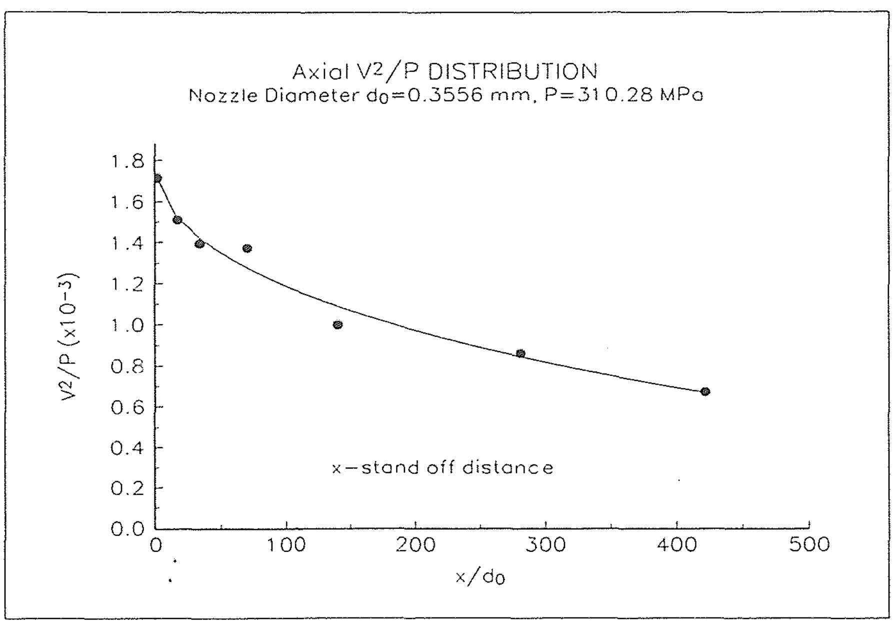

Figure 67 Axial V^2/P distribution for nozzle diameter of 0.3556 mm under pressure of 310.28 MPa

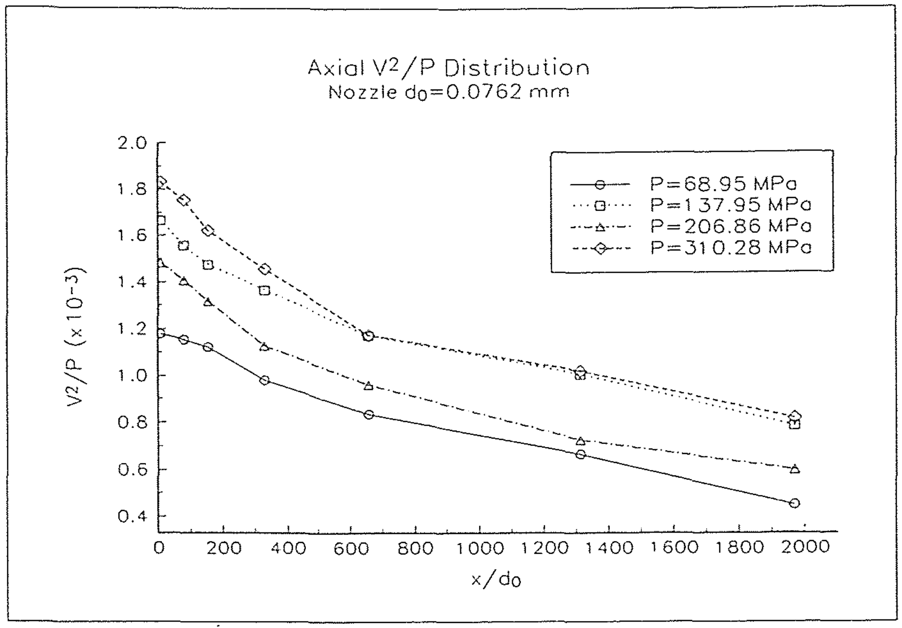

Figure 68 Axial V^2/P distribution for nozzle diameter of 0.0762 mm under different pressures

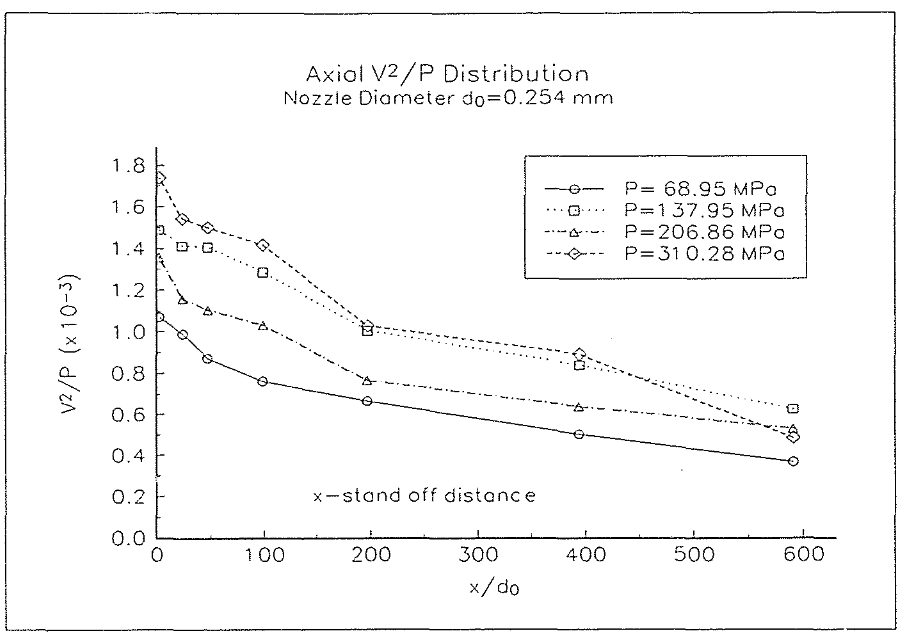

Figure 69 Axial V^2/P distribution for nozzle diameter of 0.254 mm under different pressures

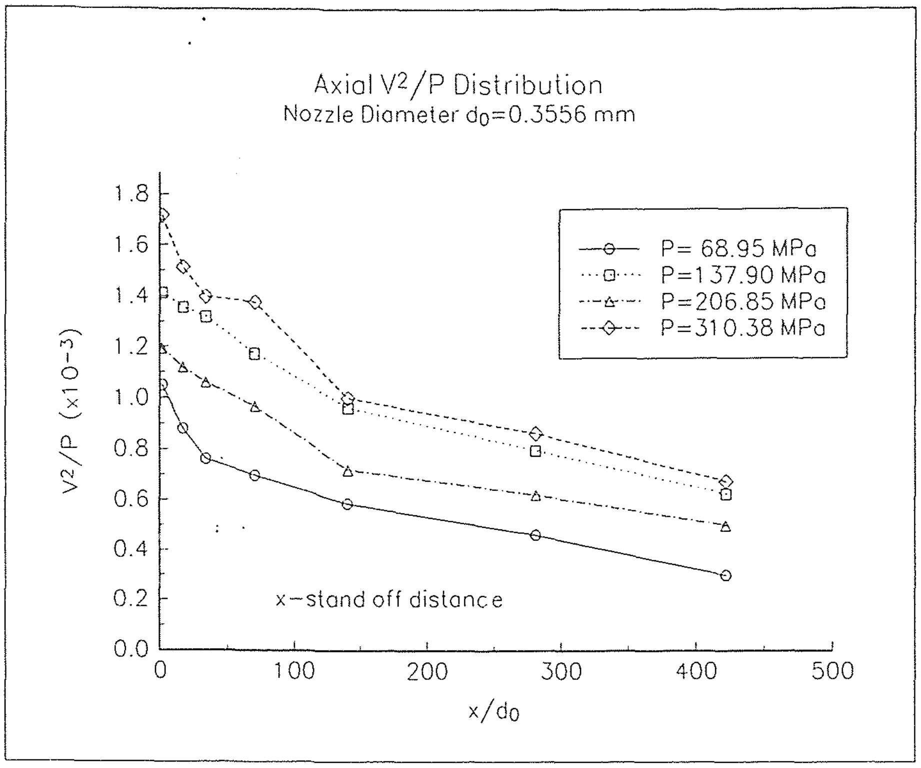

Figure 70 Axial V^2/P distribution for nozzle diameter of 0.3556 mm under different pressures

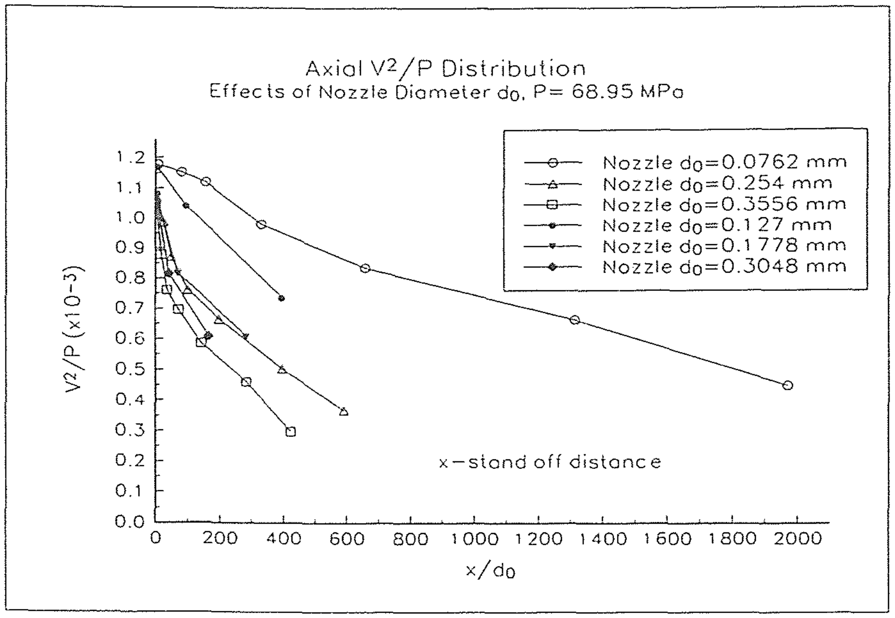

Figure 71 Axial V^2/P distribution for different nozzle diameter under pressure of 68.95 MPa

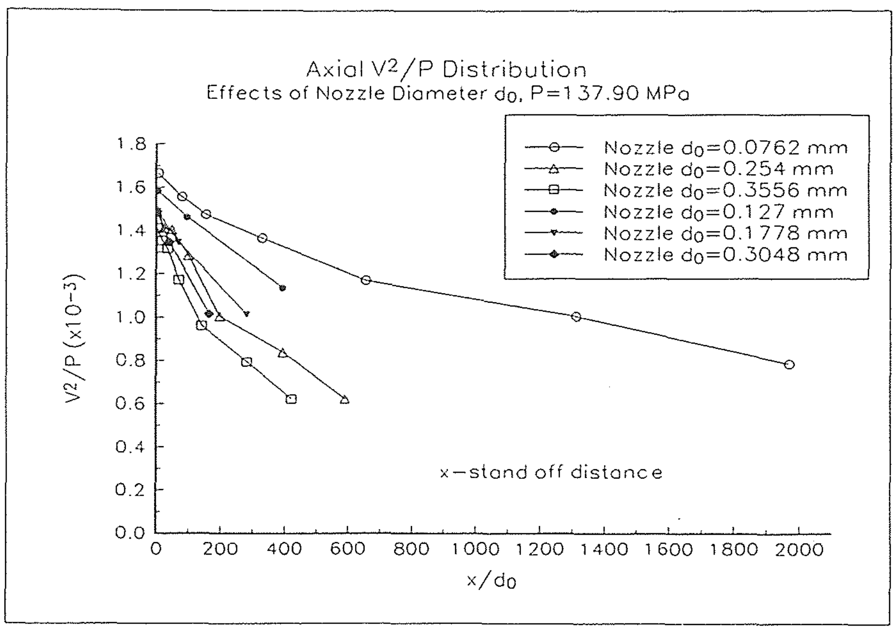

Figure 72 Axial V^2/P distribution for different nozzle diameter under pressure of 137.90 MPa

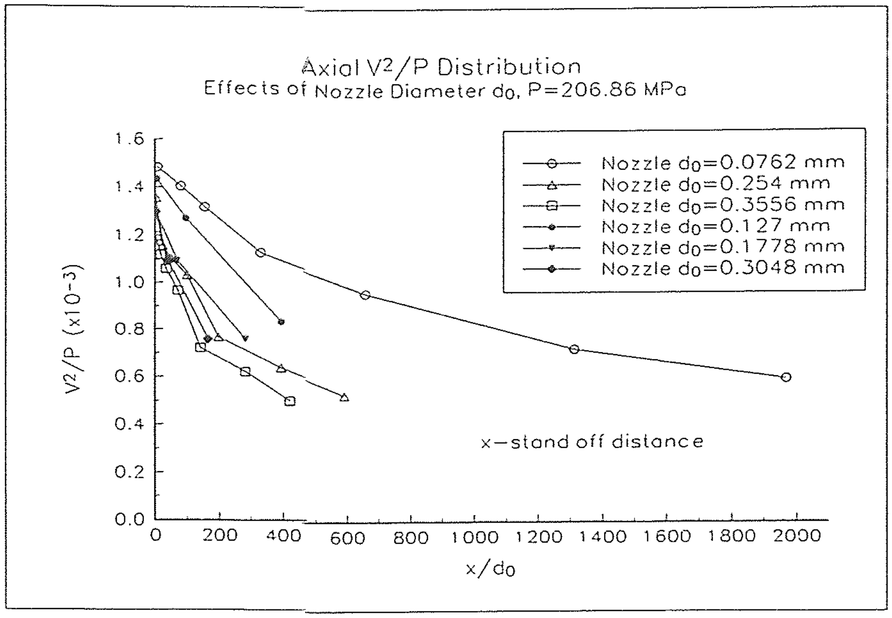

Figure 73 Axial V^2/P distribution for different nozzle diameter under pressure of 206.86 MPa

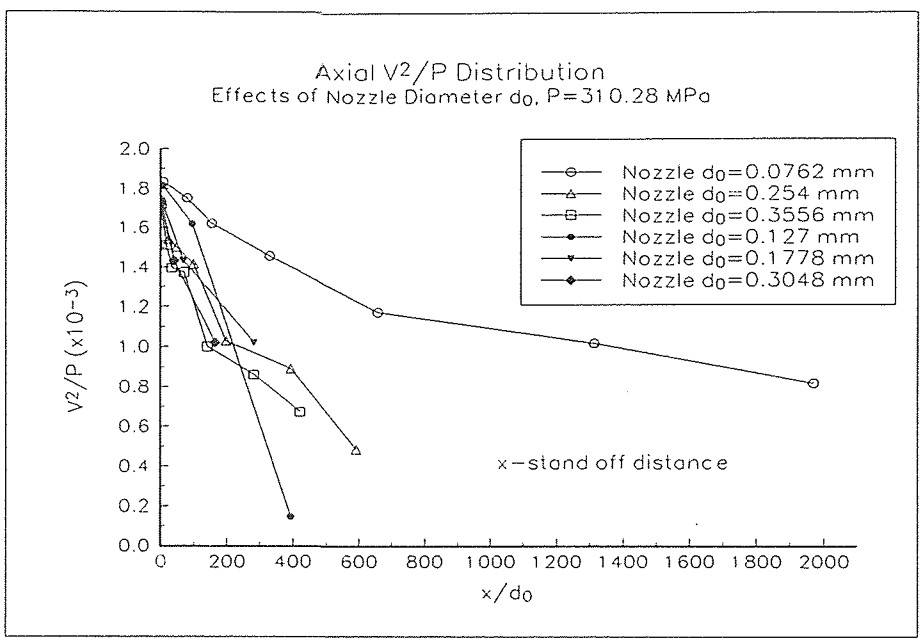

Figure 74 Axial V^2/P distribution for different nozzle diameter under pressure of 310.28 MPa

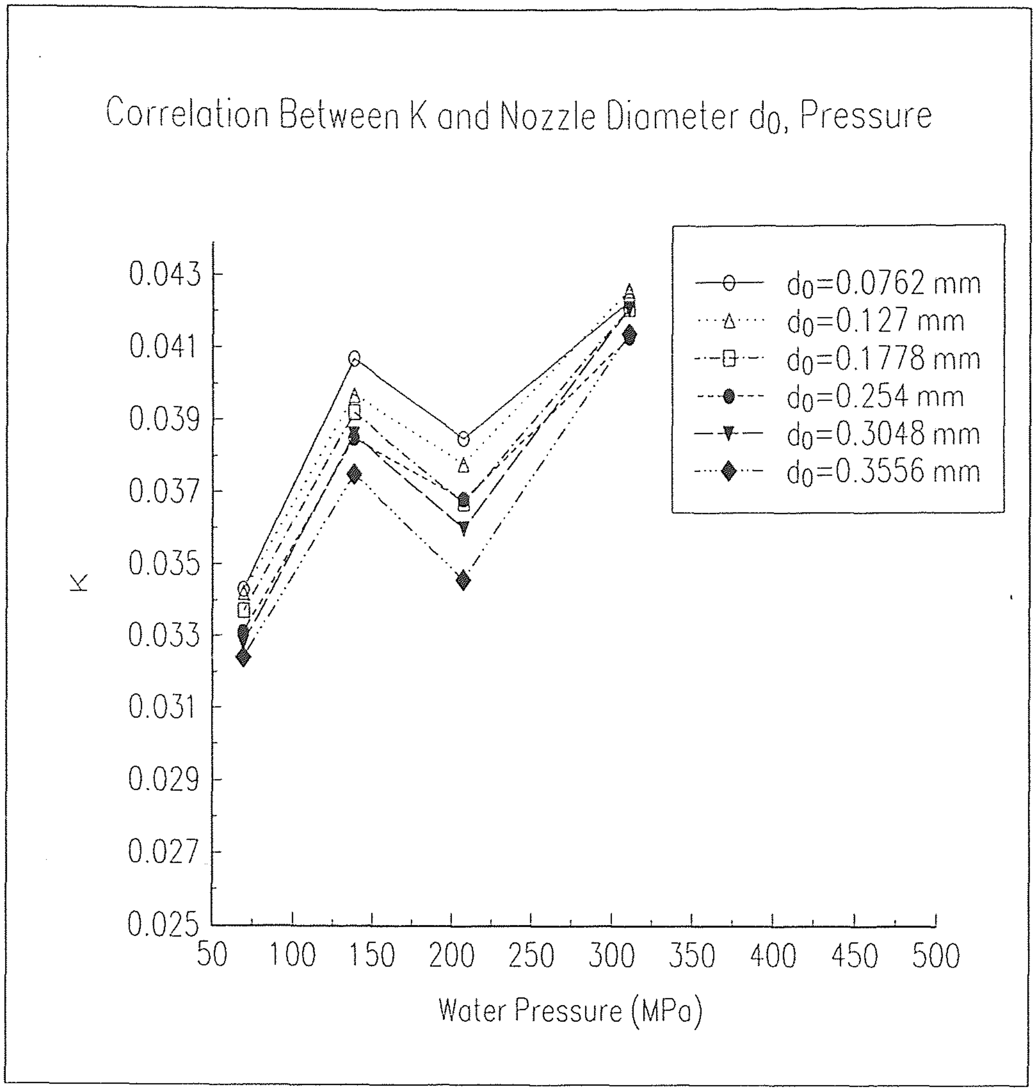

Figure 75 Correlation between K and nozzle diameter and water pressure

REFERENCES

1. DANTEC 57D 10/57 D11 Power Supply Instruction & Service Manual, 1986.

2. DISA 55X Modular LDA Optics Instruction & Service Manual, 1986.

3. DANTEC 55L90a LDA Counter Processor Instruction & Service Manual, 1986.

4. NICOLET NIC-320 Oscilloscopes Operation Manual, 1992.

5. Chen, Wei-Long. "Correlation Between Particles Velocities And Conditions of Abrasive Waterjet Formation." Ph.D Dissertation, ME Department, New Jersey Institute of Technology, December, 1989.

6. Khan, MD. Ekramul Hasan. "An Investigation of The Dynamics of Abrasive Waterjet Formation." MS Thesis, ME Department, New Jersey Institute of Technology, December, 1990.

7. Yanaida, K. and Ohashi, A. "Flow Characteristics of Water Jets in Air." *The 4th Internatonal Symposium on Jet Cutting Technology* (1978): A3-39.

8. Hishida, K., Nakano, H. and Maeda, M. "Turbulent. Flow Characteristics of Liquid-Solid Particle Confined Jet." *International Conference on Mechanics of Two-Phase Flows*, National Taiwan University, Taiwan (1989): 207-214.

9. Givler; R.C. and Mikatarian, R.R. "Numerical Simulation of Fluid Particle Flows: Geothermal Drilling Applications." *Transactions of the ASME J. of Fluid Engineering* Vol. 109 (1987): 324-331.

10. Swanson, R.K. Kilman, M., Cerwin, S. and Tarver, W. "Study of Particle Velocities in water Driven Abrasive Jet Cutting." *Proceeding. of 4th U.S. water Jet Conference* (1987): 103-107.

11. Edwards, D.G., Smith, R.M. and Farmer, G. "The Coherence of Impulsive water Jet." *The 9th International Symposium on Jet Cutting Technology* (1982): c4.123-c4.140.

12. Davies, T.W., Metcalf, R.A. and Jackson, M.K. "The Anatomy and Impact Characteristics of Large Scale Waterjets." *The 5 th International Symposium on Jet Cutting Technology* (1980): A2.15-A2.32.

REFERENCES
(Continued)

13. Janakiram, K.S. and Rao, S. B.C. "Studies of the Characteristics of Flow and Erosion due to Plain and Cavijet Impingement." *Proceeding 5th International Conference on Ersion by Solid and Liquid Impact* (1980): 70.1.-70.9.

14. Miller, AL. and Archibald, John H. "Measurement of Particle Velocity In An Abrasive Jet Cutting System" *Proceeding of 6th American Waterjet Technology Conference* (1991): 291-304.

15. Lading, L. "Estimating Time and Time-Lag in Time-of-Flight Velocimetry." *Applied Optics*, Vol. 22, No. 22 (1983): 3637-3643.

16. Loh, Y. and Tan, H. "A New Method for Processing the Signals from a Laser-Dual Focuse Velocimeter." *Journal of Physics E*, Vol.14, No.8 (1981): 981-984.

17. Himmelreich, U. and Riess, W. "Laser-Velocimetry Investigation of The Flow In Abrasive Water Jets With Varying Cutting Head Geometry." *Proceeding of 6th American Waterjet Technology Conference* (1991): 355-369.

18. Dunne, B and Cassen, B. "Velocity Discontinuity Instability of a Liquid." *Journal of Applied Physics*, Vol.27, No.6 (1956): 577-582.

19. Semerchan, A.A., Vereschagin, L.F., Filler, F.M. and Kuzin, N.N. "Distribution of Momentum in a Continuous Liquid Jet of Supersonic Velocity." *Technology Physics*, Vol.3, No.9 (1958): 1984-1903.